First-principles modeling of chlorine isotope fractionation between chloride-bearing molecules and minerals

Etienne Balan, Laura Créon, Chrystèle Sanloup, Jérôme Aléon, Marc Blanchard, Lorenzo Paulatto, Hélène Bureau

First-principles modeling of chlorine isotope fractionation between chloride-bearing molecules and minerals

Etienne Balan[1], Laura Créon[1], Chrystele Sanloup[1], Jérôme Aléon[1], Marc Blanchard[2], Lorenzo Paulatto[1], Hélène Bureau[1]

[1]Sorbonne Université, CNRS, IRD, MNHN, Institut de Minéralogie, de Physique des Matériaux et de Cosmochimie (IMPMC), 4 place Jussieu, 75252 Paris cedex 05, France
[2]Géosciences Environnement Toulouse (GET), Observatoire Midi-Pyrénées, Université de Toulouse, CNRS, IRD, UPS, 14 avenue E. Belin, 31400 Toulouse, France

Keywords : Cl isotopes, first-principles modeling, brines, Cl-bearing minerals, solar nebula

Abstract

Equilibrium $^{37}Cl/^{35}Cl$ fractionation factors in selected molecules, Cl-bearing crystalline solids, and silicates in which Cl occurs at trace or minor concentration level are determined from first-principles calculations, within the density functional theory (DFT) scheme. Results on benchmarking molecules and crystalline solids are consistent with the previous theoretical study of Schauble et al. (2003). The present study further documents the control of the isotopic fractionation properties of chlorine by its local bonding environment. Chloromagnesite and chlorapatite display similar isotopic fractionation properties due to relatively similar bonding environment. In contrast, trace Cl in Mg-serpentine (lizardite) and Mg-amphibole (anthophyllite) are enriched in ^{37}Cl with respect to chloromagnesite, due to the structural constraints exerted by the host structure on the substituted ion. This effect is even more pronounced when Cl is associated to hydroxylated cationic vacancies in forsterite. An effect of the local bonding environment on the Cl isotopic fractionation properties is also inferred for Cl^- ions in saturated aqueous solutions. It explains the systematic departure between theoretical and empirical reduced partition function ratio observed for the alkaline chlorides, differing from the agreement observed for the hydrated Cl salts. The reduced partition function ratio of Cl^- ions in concentrated solution of alkaline chlorides is smaller from that observed in dilute solutions by an amount potentially reaching 1‰ at 22°C. Finally, the calculation of fractionation factors between gas ($HCl_{(g)}$, $NaCl_{(g)}$, $KCl_{(g)}$) and solids (sodalite, chlorapatite, halite, HCl trihydrate) which likely prevailed in the solar nebula, sustains a model in which the ^{37}Cl enrichment of $HCl_{(g)}$ is produced by a Rayleigh type fractionation during chlorine condensation at temperatures between 400 and 500 K.

This model could explain the heavier isotopic composition observed for bulk Earth and various chondrites compared to the nebular gas.

1. Introduction

The $^{37}Cl/^{35}Cl$ isotopic composition of chlorine in major Earth's reservoirs (seawater, evaporites, mantle) exhibits a limited range of values, with most of them falling between -0.5 ‰ and +0.5 ‰ from the seawater composition (Eggenkamp, 2014; Barnes and Sharp, 2017). Strong departures from these values are most often ascribed to non-equilibrium kinetic processes affecting the Cl isotopic composition, which include Cl loss during degassing processes (Sharp et al., 2010a,b) as well as diffusion and ion filtration in porous media explaining negative values of sedimentary pore fluids (e.g. Godon et al., 2004). At a larger scale, degassing processes are expected to explain the heavier isotopic composition of planetary reservoirs, such as the Moon or the crust of Mars, because of the preferential loss of light chlorine isotope (Sharp et al., 2010a; Barnes and Sharp, 2017; Wang et al., 2019). Equilibrium isotopic fractionation of chlorine in nature is generally expected to be of smaller magnitude because chlorine mostly occurs under a single redox state, the reduced chloride ions, and the relative mass difference between the isotopes is small. In addition, and although equilibrium isotopic fractionation involving oxidized forms of chlorine such as perchlorates can be large (Schauble et al., 2003), the photochemical formation of these unstable species is not expected to fractionate the chlorine isotopes (Barnes and Sharp, 2017).

Few equilibrium fractionation factors of Cl isotopes have been experimentally determined. They include the $HCl\text{-}Cl^{-}_{(aq),}$ (Sharp et al., 2010b) and the $Cl_2\text{-}Cl^{-}_{(aq)}$ (Giunta et al., 2017) fractionation coefficients at near-ambient conditions; as well as fractionation between chloride salts and saturated solutions (Eggenkamp et al., 1995, 2016). At high temperature, Sharp et al. (2007) reported a -0.3 ‰ fractionation factor between sodalite and $NaCl_{(l)}$ at 825 °C and Cisneros (2013) documented a +0.1 ‰ fractionation

74 factor between amphibole and NaCl-bearing solution at 700°C and 0.2 GPa. Observations
75 made on seafloor serpentinite and altered oceanic crust also point to a small positive
76 serpentine-$Cl^-_{(aq)}$ and amphibole-$Cl^-_{(aq)}$ fractionation.

77 Theoretical isotopic fractionation factors between molecular species and
78 crystalline chlorides have been predicted by combining experimentally observed
79 vibrational frequencies and theoretically predicted frequency shifts due to the isotopic
80 substitution (Schauble et al., 2003). For molecules, theoretical predictions were based
81 on ab-initio quantum-mechanical calculations, whereas those for crystalline solids made
82 use of empirical force-fields. This set of theoretical fractionation coefficients revealed
83 significant equilibrium enrichment in ^{37}Cl in oxidized chlorine species as well as in Cl-
84 bearing organic molecules. The fractionation between more reduced Cl_2 and HCl
85 molecules was found to be consistent with experimental data and the role of the local
86 environment of chloride ions in minerals was underlined, suggesting enrichment of
87 silicates in ^{37}Cl with respect to simple Na, K or Rb chlorides (Schauble et al., 2003). More
88 recently, Schauble and Sharp (2011) reported a -0.7 ‰ fractionation between sodalite
89 and HCl at 950 K and a -0.02 ‰ fractionation between sodalite and $NaCl_{(c)}$ at 1098 K.
90 They also predicted a +3 to +6 ‰ fractionation between crystalline HCl hydrate and
91 $HCl_{(g)}$ at 140-160 K, a fractionation potentially explaining the variability of Cl isotopic
92 composition observed in chondrites (Sharp et al., 2013; Gargano et al., 2017).

93 Previous studies have shown that theoretical fractionation factors computed
94 from first-principles within density functional theory (DFT) provide useful information
95 on isotopic systems that are difficult to address on a purely experimental basis because
96 they involve, e.g., uncommon isotopic effects (Schauble et al., 2006), slow chemical
97 reactions (Méheut et al., 2007), weakly fractionating isotopes (Blanchard et al., 2009;
98 Moynier et al., 2011; Blanchard et al., 2017), incorporation of minor or trace elements in

minerals (Rustad and Zarzycki, 2008; Balan et al., 2018) or high-temperature reactions between solids and dilute gas (Javoy et al., 2012). In the present work, we apply this approach to chlorine isotopes by providing a set of theoretical fractionation factors between selected molecules (Table 1) and crystalline solids (Table 2) in which chlorine occurs as a major or a trace element, all systems being treated at the same theoretical level. This study mostly focuses on chloride, the lowest redox state of chlorine, which corresponds to the most frequently observed in natural systems. The investigated phases include cosmochemically important molecules, ($HCl_{(g)}$, $NaCl_{(g)}$ and $KCl_{(g)}$), Cl-bearing minerals (chlorapatite, sodalite, chloromagnesite and Cl salts precipitating from aqueous solutions), as well as rock-forming silicates displaying Cl as a trace element (lizardite, anthophyllite, forsterite).

2. Methods

2.1. Expression of isotopic fractionation factors

Assuming a system with two stable isotopes, the equilibrium isotopic fractionation coefficient of an element Y between two phases a and b, referred to as $\alpha(a,b,Y)$, is defined by the isotopic ratios:

$$\alpha(a,b,Y)=(Y^*/Y')_a/(Y^*/Y')_b \quad (1)$$

where Y* and Y' are the abundances of the two different isotopes. Accordingly, it can be related to the equivalent coefficients, referred to as β-factors, obtained for each phase and a reference system corresponding to an ideal gas of Y atoms:

$$10^3 \ln \alpha(a,b,Y) = 10^3 \ln \beta(a,Y) - 10^3 \ln \beta(b,Y) \quad (2)$$

The β(a,Y) factor is related to the reduced partition function ratio of the isotopomers and harmonic expressions have been derived for molecular systems by Bigeleisen and Mayer (1947). Using the high-temperature product (Redlich-Teller) rule, the harmonic β-factor of a diatomic molecule is given by:

$$\beta(a,Y) = \frac{\nu^*}{\nu} \frac{e^{-h\nu^*/(2kT)}}{1-e^{-h\nu^*/(kT)}} \frac{1-e^{-h\nu/(kT)}}{e^{-h\nu/(2kT)}} \quad (3)$$

were ν and ν* are the harmonic stretching frequencies of molecules differing by a single isotopic substitution, *k* the Boltzmann constant, *h* the Planck constant, and T the temperature. This expression is valid for molecules containing more than a single Y atom provided that the isotopic mixing is ideal, a verified assumption in the case of chlorine isotopes (Schauble et al., 2003).

For a crystal, harmonic β-factors can be calculated in a similar way using the following expression:

$$\beta(a,Y) = \left[\prod_{i=1}^{3N_{at}} \prod_{\{q\}} \frac{\nu_{q,i}^*}{\nu_{q,i}} \frac{e^{-h\nu_{q,i}^*/(2kT)}}{1-e^{-h\nu_{q,i}^*/(kT)}} \frac{1-e^{-h\nu_{q,i}/(kT)}}{e^{-h\nu_{q,i}/(2kT)}} \right]^{1/(NqN)} \quad (4)$$

where $\nu_{q,i}$ are the frequencies of the phonon with wavevector q and branch index i = 1,3N_{at}. N_{at} is the number of atoms in the unit cell, $\nu_{q,i}$ and $\nu^*_{q,i}$ are the vibrational

frequencies in two isotopically different materials, N is the number of sites for the Y atom in the unit cell (e.g., Méheut et al., 2007). In the product over the N_q q-vectors of Eq. (4), the three translational modes at the center of the Brillouin zone with $\nu_{0,i} = 0$ are not considered. The β-factors can thus be calculated for molecules and crystalline solids using Eq. (3) and (4) and vibrational frequencies calculated from first-principles.

The calculation of the whole vibrational spectrum is sometimes prevented by the too large size of the considered system. In this case, a useful approximation can be used to obtain the β-factor from the restoring force constants F_i corresponding to the displacement of the isotopic atom in three mutually perpendicular directions (Bigeleisen and Mayer, 1947; Moynier et al., 2011; Ducher et al., 2017):

$$\beta \approx 1 + \frac{M' - M}{M'M} \frac{h^2}{96\pi^2 k^2 T^2} \sum_{i=1}^{3} F_i \qquad (5)$$

where M and M' are the masses of the two isotopes.

2.2 Computational details

Relevant vibrational properties, i.e. phonon frequencies (Eq. 3 and 4) or restoring force constants (Eq. 5), were obtained within the density functional theory (DFT) framework, using the generalized gradient approximation (GGA) to the exchange-correlation functional as proposed by Perdew, Burke and Ernzerhof (PBE; Perdew et al., 1996) and a plane-wave / pseudopotential scheme, as implemented in the PWscf and PHonon codes from the Quantum-Espresso package (Baroni et al., 2001; Giannozzi et al., 2009; http://www.quantum-espresso.org). The ionic cores were described using optimized norm-conserving Vanderbilt (ONCV) pseudopotentials (Hamann, 2013;

Schlipf and Gigy, 2015) with 80 and 480 Ry cut-offs on the electronic wave functions and charge density, respectively, ensuring that total energies are converged within 1 mRy/atom. Before the computation of vibrational properties, the relaxation of atomic internal coordinates was performed until the residual forces were less than 10^{-4} Ry/au. Initial guess of mineral structures were built using the experimental data (Table 2) obtained from the American Mineralogist Crystal Structure Database (Downs and Hall-Wallace, 2003). To compute the properties of isolated molecules (Table 1), a single molecule was inserted in a cubic box with cell parameter a = 15.87 Å, a size large enough to marginalize the interactions between periodic images of the molecule. In this case, the electronic integration was performed by restricting the Brillouin-zone sampling to a single k-point. For minerals, k-point grids are reported in Table 2 and both the cell-parameters and atomic positions were relaxed under zero pressure. Depending on the system size a finite grid of q-points (Eq. 4) or the force-constant approximation (Eq. 5) were used to compute the β-factors (Table 2). In the finite grids of q-vectors (Eq. 4), the center of the Brillouin zone (Γ point) was not included.

2.3 Structural models of Cl incorporation in silicates at trace or minor concentration level

Chlorine usually occurs in rock-forming minerals as a trace or minor element. Hydrous phyllosilicates and amphiboles are able to incorporate chlorine up to the wt. % level. These significant concentrations are explained by the possibility to substitute chloride ions for structural OH groups in these hydrous minerals (Volfinger et al., 1985). Oceanic serpentines can contain up to 6200 ppm Cl (e.g. Scambeluri et al., 2004) and are considered as key actors of Cl recycling in the mantle (Kendrick et al., 2011).

Accordingly, periodic models of Cl-bearing lizardite ($Mg_3Si_2O_5(OH)_4$) and anthophyllite ($Mg_7Si_8O_{22}(OH)_2$) have been considered for their relative chemical simplicity. In order to minimize, as much as possible, spurious interactions between the periodic images of the substituted chloride ions, the unit-cell of the periodic Cl-bearing lizardite model has been built from a 2x2x2 supercell containing 112 atoms. Two different lizardite models were considered, referred to as Cl1 and Cl2, corresponding to Cl substitution for an inner-OH or an inter-layer OH group, respectively. The anthophyllite cell also contains two non-equivalent OH-groups leading to two different models, referred to as Cl1 and Cl2. The local environment around the two OH-groups is however more similar than in lizardite. In anthophyllite, the primitive cell contains 164 atoms and it was not possible to handle a larger supercell. The distance between Cl in neighboring cells is 5.27 Å along the c direction. As the structure is constrained along this direction by the silicate chains, we expect that the local structure around chlorine ions, and therefore their isotopic fractionation properties, is weakly affected by the presence of the chlorine ions in neighboring cells.

The incorporation mechanisms of halogens in olivine are still debated, despite its potentially important role in the storage of halogens in the upper mantle (Beyer et al., 2012; Dalou et al., 2012; Joachim et al., 2015; 2017). Several studies have pointed out the key role of hydroxylated defects in the incorporation of fluorine in forsterite, the Mg olivine end-member (Crépisson et al., 2014; Joachim et al., 2015). Compared with fluorine, partition coefficients of chlorine between olivine and melt are smaller, with a lower dependence on the olivine water content (Joachim et al., 2017). Nonetheless, in absence of definite conclusions concerning the incorporation mechanism of chlorine in olivine, we considered that the Cl for OH substitution in hydroxylated defects of olivine still is a viable incorporation mechanism. Other mechanisms involving, e.g. the charge

compensation of cationic vacancies by the association of several chloride ions in a single defect, does not seem to be more favorable because of the low Cl concentration. Accordingly, two types of models of hydroxylated defects, related to Si or Mg vacancies in forsterite, were considered as potential candidates for the structural incorporation of chloride ions. These models have been built from a 2x1x2 forsterite supercell and previously validated by comparison with infrared spectroscopic observations (Balan et al., 2011; 2017). In these models, only one Cl atom has been substituted for one of the OH groups. In the case of the hydroxylated Si vacancy, three non-equivalent OH groups can be substituted, leading to three Cl-bearing forsterite models referred to as Si_Cl1, Si_Cl2 and Si_Cl3 (Table 3), where the number corresponds to the substituted hydroxyl and the configuration is identical to that of the fluorinated models investigated by Crépisson et al. (2014). An additional model (Si_Cl1b) was considered, corresponding to a configuration in which the O2-H group points toward the neighbouring vacant site as in the hydroxylated Si vacancy model described in Balan et al. (2017). Five models preserving the electrostatic charge neutrality can be built for the hydroxylated Mg vacancy (Table 3).

The equilibrium geometry of Cl-poor silicates was obtained by displacing all atoms up to a minimum energy state, characterized by the fact that the forces experienced by the atoms vanish. During this relaxation, the cell geometry was kept fixed to that of the pure phase, as previously done in e.g. Balan et al. (2014) or Crépisson et al. (2018).

3. Results

3.1 Benchmarking the modeling approach

The first-principles calculation of isotopic fractionation factors relies on a number of approximations which can introduce systematic bias in the computed values of β-factors. The stronger approximations rely on the use of the harmonic approximation and in the choice of the exchange-correlation functional, here the PBE functional. As observed in previous studies, the PBE calculations tend to overestimate bond lengths and crystal cell-parameters by typically 1 to 2 % (Table 1 & 2). The agreement is slightly poorer for chlorapatite, with a stronger overestimation of the *a* cell-parameter and a slight contraction of the *c* cell-parameter (Table 1). Similar distortion of the cell geometry was observed in previous modeling of the properties of F- and OH-apatite at the GGA level (Corno et al., 2006; Balan et al., 2011b; Aufort et al., 2018). An overestimation of the *c* cell-parameter of chloromagnesite is also observed. It is likely related to the dominant Van der Waals contribution to the cohesion energy of the layered chloromagnesite structure, a contribution which is not accounted for by the PBE functional. Similar overestimation is observed in other layered minerals displaying non hydrogen-bonded neutral layers, such as talc. It is however not expected to strongly affect the vibrational properties of the structure as the layer geometry is preserved (Blanchard et al. 2018). Significant differences between theory and experiment are also observed in the cell geometry of the hydrated salts bischofite ($MgCl_2.6(H_20)$) and $BaCl_2.2(H_20)$ (Table 2). The structure of bischofite displays $Mg(OH_2)_6^{2+}$ polyhedra sharing H-bonds with neighboring Cl^- ions or H_2O molecules; whereas the hydrated barium dichloride displays layers of edge sharing $Ba(OH_2)_4Cl_4$ polyhedra. In such type of molecular edifices, the neglect of Van der Waals interactions and thermal effects related to the anharmonicity of weak H-bonds could be stronger than in crystals whose cohesion is ensured by iono-covalent bonding.

The properties of small molecules (HCl, Cl_2) and simple chloride salts (Table 1 & 2) can be compared to their experimental counterparts and to previous calculations by Richet et al. (1977) and Schauble et al. (2003) (Fig. 1). As expected, the systematic overestimation of bond distances and cell parameters due to the GGA, leads to an underestimation of vibrational frequencies by ~5% (Fig. 2). The difference is however larger for $CsCl_{(c)}$ than for the other halides, reaching 25% despite similar agreement between theoretical and experimental cubic cell parameters (Table 2). A modeling of CsCl using a different exchange-correlation functional (PBEsol; Perdew et al., 2008) provided a smaller *a* cell-parameter (4.06 Å), increasing the zone-center TO frequency to 93.5 cm^{-1} and the β-factor at 22°C by 0.43 ‰. For the molecules, a systematic ~0.5 ‰ decrease of β-factor at 0°C with respect to the previously calculated values is observed (Fig. 1). The equilibrium fractionation factor between Cl_2 and halite at 0°C is 4.6 ‰, very close to the 4.75 ‰ value computed by Schauble et al. (2003). Similarly the halite-sylvite fractionation at 0°C is 0.9 ‰ both in the present study and that of Schauble et al. (2003), confirming that systematic bias tend to compensate when combining β-factors computed at the same theoretical level.

As mentioned in the Method section, the whole vibrational spectrum is hardly obtained for systems having a large number of atoms in their unit-cell. In this case, it can be useful to use an approximate expression that relates the β-factor to the restoring force constant when the relevant atom is displaced from its equilibrium position (Eq. 5). This approximation of the harmonic expression of the reduced partition function ratio assumes that the force-constants are isotope-independent. It is valid when the ratio of the relevant vibrational frequencies to the temperature and the relative mass difference between the isotopes are sufficiently small (Blanchard et al., 2017). Accordingly, the use of the force-constant approximation was tested on the forsterite_Si_ Cl1 model. This

295 model displays a relatively high β-factor indicating that the relevant vibrational
296 frequencies are among the highest observed among the investigated systems. The
297 comparison between the β-factor obtained using the full expression (Eq. 4) and the
298 approximate one (Eq. 5) indicate that for a temperature above 450 K, the difference is
299 smaller than 0.1 ‰. As the force constant approximation is obtained from a finite
300 expansion of the full harmonic expression of the β-factor, the quality of the
301 approximation is better for systems displaying smaller vibrational frequencies and
302 related smaller β-factor. For example, the difference between the force constant
303 approximation and the full calculation for the NaCl and KCl molecules is smaller than 0.1
304 ‰ at 298 K.
305
306 *3.2 Local environment and isotopic β-factor of chloride in condensed phases*
307
308 The isotopic fractionation properties of chlorine reflect its local bonding
309 environment. For all the investigated solid phases, the temperature dependence of the
310 reduced partition function ratios is mostly linear and the corresponding slope
311 coefficients are given in Table 4. In monochloride salts, chlorine displays a coordination
312 varying from 8 in CsCl to 6 in the other chlorides with halite structure. The
313 corresponding reduced partition function ratio at 22°C (Table 5) display a systematic
314 variation as a function of the cation ionic radius, the larger cations leading to smaller β-
315 factors (Fig. 3). In the hydrated Mg, Ca and Sr dichloride salts, the chloride ion is bonded
316 to water molecules belonging to the coordination sphere of the cations (Table 3).
317 Consistently, these phases display similar β-factors, not correlated with the cation
318 radius (Fig. 3). In the peculiar HCl tri-hydrate structure, the HCl molecule is dissociated
319 and the chloride ions are surrounded by Zündel ions ($H_5O_2^+$) (Lundgren and Olovsson,

320 1967). The corresponding β-factor is larger than that observed in the hydrated
321 dichloride salts in which chloride ions are surrounded by water molecules (Table 4).
322 When solely bound to divalent cations, chlorine displays a three-fold
323 coordination. This environment is observed in chloromagnesite and chlorapatite, as well
324 as in the silicates anthophyllite and lizardite. The β-factor of chloromagnesite (6.2 ‰ at
325 0°C) is consistent with the values reported for the isostructural compounds $FeCl_2$ and
326 $MnCl_2$ (6.7 and 6.2 ‰ at 0°C, respectively) by Schauble et al. (2003). Despite an
327 apparently similar environment and Mg-Cl distances close to 2.5 Å, the β-factor of Cl-
328 sites in lizardite and anthophyllite are significantly higher than that of chloromagnesite
329 (Table 4, Fig. 4). This suggests that the environment of Cl atoms is more constrained
330 when Cl is incorporated as a substituting element in silicates than when it occurs as a
331 major constituent of the mineral. As a matter of fact, the Mg-Cl-Mg angle decreases from
332 93 ° in chloromagnesite to about 80° in lizardite and anthophyllite. The effect of the host
333 structure on the vibrational and isotopic fractionation properties of Cl is even stronger
334 when considering the Cl sites in forsterite. In the case of the defects related to Si
335 vacancies, the Mg-Cl distances are smaller than in the chloride minerals (Table 3).
336 Neighboring OH groups can also point toward the Cl ion, suggesting a weak additional
337 bonding to H atoms. For the defects related to Mg vacancies, Cl ions are bound to Si
338 atoms and the largest β-factors are observed. Although it is not possible to directly
339 compare the energy of chemically different incorporation mechanisms, it can be noticed
340 that the less stable configurations of a given defect are observed for the environments
341 leading to the shortest Cl-cation distances (Table 3).
342 Finally, chloride ions in sodalite display a lower 4-fold coordination states with
343 bonding to Na atoms. Compared with halite, the lowering of the coordination state is
344 balanced by a shortening of the Cl-Na bond leading to a very similar β-factor for both

345 minerals. The calculated fractionation factor between HCl and sodalite (0.7 ‰ at 950 K)
346 is in excellent agreement with the value proposed by Schauble and Sharp (2011).
347
348 **4. Discussion**
349
350 *4.1 Chlorine isotope fractionation during precipitation from saturated solutions*
351
352 The precipitation of chloride salts from concentrated aqueous solutions is an
353 important natural process leading to the formation of evaporitic rocks. The equilibrium
354 isotopic fractionation factors of chlorine between aqueous solutions and precipitating
355 NaCl, KCl and hydrated $MgCl_2$ has been experimentally determined by Eggenkamp et al.
356 (1995). The moderate values, varying between +0.26 ‰ and -0.08 ‰ for $NaCl_{(c)}$ and
357 $KCl_{(c)}$, respectively, were found to be roughly consistent with the theoretical values
358 provided by Schauble et al. (2003). Although debated (Luo et al., 2014, 2015;
359 Eggenkamp et al., 2015), the initially proposed experimental values have been more
360 recently confirmed by Eggenkamp et al. (2016). This series was also complemented by
361 the experimental determination of fractionation factors between aqueous solutions and
362 Li, Cs, Rb, Ca and Sr salts (Eggenkamp et al., 2016). The comparison of theoretical
363 results with experimental fractionation factors is not straightforward because theory
364 only provides β-factors within a given level of approximation. Although fractionation
365 factors and β-factors are simply related by Eq. (2), the theoretical prediction of
366 equilibrium isotopic fractionation between solids and solutions is hampered by
367 computational constraints which make it difficult to treat the liquid and solid phases at
368 the same approximation level (Blanchard et al., 2017). Using an empirical electrostatic
369 model of ion solvation by water molecules, Czarnacki and Halas (2012) have computed

370 the β-factor of the aqueous chloride ion. Combined with the β-factor of the Cl_2 molecule
371 computed by Schauble et al. (2003), a good agreement was observed between the
372 theoretical values and the experimental fractionation factor between Cl_2 vapor and
373 aqueous chloride ions determined by Giunta et al. (2017). This suggests that the β-factor
374 determined by Czarnacki and Halas (2012) can account for equilibrium fractionation
375 properties of chloride in real aqueous solutions. Thus, the β-factor of the salts can be
376 empirically assessed from Eq. (2), assuming that the reduced partition function ratio of
377 aqueous chloride calculated by Czarnacki and Halas (2012) (1000ln(β)=3.13 ‰ at 22
378 °C) matches that of saturated solutions and using the fractionation factors determined
379 by Eggenkamp et al. (2016). Similarly, the β-factor of the Cl_2 molecule can be obtained
380 using the experimental data of Giunta et al. (2017). The comparison of these empirical β-
381 factors with the present theoretical ones reveal a high level of consistency for the Cl_2
382 molecule and the hydrated Li, Mg, Ca and Sr salts, with a minor theoretical
383 underestimation of the β-factors most likely due to the systematic bias related to the
384 PBE functional (Fig. 5). A more pronounced departure is observed for cubic salts (NaCl,
385 KCl, RbCl, CsCl) and hydrated $BaCl_2$, with the empirical values being systematically
386 larger than the theoretical ones. The observed difference is always above 0.5 ‰ and can
387 reach 1.5 ‰ for CsCl. In comparison, the difference between empirical and theoretical
388 β-factors for Cl_2 molecules is only 0.14 ‰, supporting the combination of the aqueous
389 chloride β-factor computed by Czarnacki and Hallas (2012) with experimental
390 fractionation factors to infer empirical β-factors of solids and molecules. Experimental
391 measurements also provide isotopic composition values with typical errors smaller than
392 ±0.1 ‰ (Eggenkamp et al. 2016). Assuming that the experiments correspond to isotopic
393 equilibrium conditions, this suggests that the observed departure between empirical

394 and theoretical β-factors for these salts does not solely arise from theoretical or
395 experimental inaccuracies but rather reflects a variation in the β-factor of Cl^- ions in
396 concentrated aqueous solutions. The weak experimental fractionation observed
397 between brines and crystalline salts, compared to the theoretical variation of the β-
398 factor of solid phases (Fig. 3), suggests that the β-factor of Cl^- ions in concentrated
399 solutions follows the trend observed in the solids. According to the present results, the
400 β-factor of Cl^- ions in saturated solutions could be smaller than that observed in dilute
401 solutions. The observed difference is larger than 0.5 ‰ and could reach 1 ‰ for CsCl
402 (Fig. 6), taking into account the ~0.43 ‰ difference related to the lower accuracy of the
403 PBE functional to model $CsCl_{(c)}$. Potential role of ion pairing in solution was previously
404 suggested by Schauble et al. (2003) and Eggenkamp et al. (2016). Significant contact ion-
405 pairing in concentrated CsCl and RbCl solutions has been recently observed by X-ray
406 absorption fine structure (XAFS) spectroscopy and X-ray diffraction (XRD) (Pham and
407 Fulton, 2016; 2018). In contrast, $CaCl_2$ solutions are dominated by solvent-separated ion
408 pairs (Pham and Fulton, 2013; Friesen et al., 2019). Although deserving further
409 investigation, these observations consistently point to a stronger modification of the
410 local environment of chloride ions in concentrated aqueous solutions for the larger
411 alkaline cations with a smaller ionic potential.
412
413 *4.2 Chlorine isotope fractionation in rock-forming silicates*
414
415 Equilibrium fractionation of chlorine isotopes among silicate minerals is constrained by
416 few experimental measurements. Sharp et al. (2007) reported a -0.3 ‰ fractionation
417 factor between sodalite and $NaCl_{(l)}$ at 825 °C and Cisneros (2013) determined a +0.1 ‰
418 fractionation factor between amphibole and NaCl-bearing solution at 700°C and 0.2 GPa.

A fractionation of +0.33 ‰ between structurally bound and water-soluble Cl in seafloor serpentinites is documented by Sharp and Barnes (2004). A positive amphibole-$Cl^-_{(aq)}$ fractionation is also consistent with observations made on altered oceanic crust (Barnes and Cisneros, 2012) and metasomatised meta-gabbro (Kusebauch et al., 2015). Based on the similarity between the local environment of chlorine in serpentine and amphiboles and that observed in dichloride salts, a ^{37}Cl enrichment with respect to parent fluids is consistent with the theoretical constraints (Schauble et al., 2003). The present results provide twice as large β-factors of chlorine occurring as a trace or minor element in silicates as those of dichloride salts. Assuming that the Cl β-factor in high temperature fluids does not exceed the theoretical predictions for aqueous Cl (Czarnacki and Halas, 2012), they confirm the ^{37}Cl enrichment of chloride bearing silicates with respect to the parent fluids. The equilibrium isotopic fractionation between silicates and fluids remains however weak, not exceeding 2 ‰ at 400 °C.

Concerning trace chlorine occurring as defects in forsterite, the usually high formation temperature of olivine leads to very small isotopic fractionation. The fractionation factor between forsterite and halite is smaller than 0.3 ‰ at 1300 °C. Although very weak, measurement of differences in the isotopic composition of experimentally grown samples of forsterite in presence of NaCl might help to discriminate between inclusion of small halite particles and structural incorporation of chlorine. We note however that lower formation temperature (<610 °C) of Fe-rich olivine has been reported in some chondrites (Ganino and Libourel, 2017) potentially leading to larger Cl isotope fractionation.

Overall, the weakness of equilibrium isotopic fractionation factors of chlorine at high temperature cannot explain the variations observed in Middle Ocean Ridge basalts (Bonifacie et al., 2008) or olivine-hosted melt inclusions from island arcs basalts

444 (Bouvier et al., 2019). It sustains the use of Cl isotopes to identify mixing processes
445 involving more fractionated and shallow Cl reservoirs such as seawater, altered oceanic
446 crust serpentinites or sediments.
447
448 *4.3 Isotopic fractionation during Cl condensation in the solar nebula*
449
450 The behavior of Cl and related isotopic fractionation during the formation of the
451 solar system is still an open question. It was initially thought that the homogeneity of
452 isotopic composition between bulk Earth, chondritic meteorites and lightest values of
453 Moon samples reflected a nebular composition close to 0 ‰ (Sharp et al., 2007). The
454 lack of isotopic fractionation between Earth and chondrites is explained by the hydrous
455 character of silicate melts, leading to a compensation between the positive fractionation
456 between HCl and Cl dissolved in melts and the preferential loss of light isotopes during
457 HCl degassing (Sharp et al., 2010a). In contrast, the elevated $^{37}Cl/^{35}Cl$ ratio measured on
458 Moon samples is explained by NaCl(g) loss from anhydrous melts.
459 However, the Cl isotopic composition of several ordinary chondrites (Sharp et al.,
460 2013), some shergottites having preserved the Mars mantle composition (Sharp et al.,
461 2016) and several iron meteorites (Gargano et al., 2017), suggests a lighter isotopic
462 composition of the nebular gas, between -3 and -5 ‰ (Sharp et al., 2016). Starting from
463 this composition, the high-temperature condensation of chlorine, corresponding to the
464 formation of sodalite at 950 K (Fegley and Lewis, 1980; Lodders, 2003), is not expected
465 to strongly fractionate the Cl isotopes. At this temperature NaCl molecules are the
466 dominant speciation of chlorine in the nebular gas (Fegley and Lewis, 1980). Based on
467 the present calculations, $NaCl_{(g)}$ displays almost no fractionation with sodalite, whereas
468 $HCl_{(g)}$ in equilibrium with $NaCl_{(g)}$ is only 0.7 ‰ heavier. Accordingly, the significantly

heavier composition observed on various chondrites, as well as in bulk Earth, cannot be explained by high-temperature fractionation mechanisms. For this reason, Sharp et al. (2016) proposed that these heavy compositions could reflect the low-temperature (< 140K) addition of Cl as HCl hydrates formed beyond the snow line. Theoretical fractionation factors proposed by Schauble and Sharp (2011), confirmed by the present results, indicate that HCl hydrates could be enriched in ^{37}Cl by up to 3-4 ‰ at these temperatures (Fig. 7). This interpretation is consistent with the suggestion of Zolotov and Miromenko (2007) that aqueous alteration of chondrites at low-pH could reflect the incorporation of HCl hydrates at temperatures as low as 160 to 140 K. However, the postulated enrichment in ^{37}Cl of HCl hydrates would only correspond to a minor fraction of hydrates in equilibrium with a dominant fraction of HCl gas having escaped from high-temperature condensation processes and still not fully condensed at low temperature. Otherwise, mass balance implies that the isotopic composition of HCl hydrates should tend to that of the nebular gas as their low-temperature condensation proceeds. Such a low fraction of HCl condensed as hydrates is at odd with observations of protostars (Kama et al., 2015) and comet 67P/Churyumov-Gerasimenko (Dhooghe et al., 2017), indicating that up to 90% of HCl, the major Cl-bearing species in the interstellar medium is frozen as ice onto the surfaces of dust grains.

The above described scenario is strongly dependent on the assumptions made on the high-temperature condensation of chlorine. Considering the condensation model proposed by Schaefer and Fegley (2010), a different scenario of the evolution of the Cl isotopic composition in the solar nebula could be proposed. According to the thermodynamical modeling of Schaefer and Fegley (2010) and more recently of Wood et al. (2019), chlorine condensates at a lower temperature, starting by forming chlorapatite at 470K by reaction of previously formed whitlockite or fluorapatite with

494 $HCl_{(g)}$ up to about 40% of total chlorine, and ending by the condensation of halite
495 directly from HCl gas at temperatures below 420K. Such lower condensation
496 temperature of chlorine is also consistent with the recent reevaluation of chlorine
497 during Earth accretion by Clay et al. (2017). New measurements of Cl concentration in
498 carbonaceous, enstatite and primitive ordinary chondrites reveals that a lower
499 condensation temperature of chlorine, close to 500 K, would be consistent with the
500 general trend observed for the other volatile elements. Based on the present results,
501 $HCl_{(g)}$, which is the dominant Cl-bearing constituent of the nebular gas at these
502 temperatures (Schaefer and Fegley, 2010), is enriched by 0.7 ‰ with respect to
503 chlorapatite at 470K and 1.7 ‰ with respect to halite at 420K (Fig. 8). At these
504 temperatures, it is reasonable to assume that the solid grains were isolated from the gas
505 and do not re-equilibrate with the gas, sustaining a Rayleigh fractionation model in the
506 absence of volatilization. In its simplest expression, this model describes the evolution of
507 the $^{37}Cl/^{35}Cl$ ratio R of the remaining $HCl_{(g)}$ as a function of the condensed fraction of
508 mineral phase *f*:

509 $$\frac{R}{R^\circ} = f^{(\alpha-1)} \quad (6)$$

510 where R° is the initial ratio of the nebular gas and α the fractionation factor between the
511 gas and the condensed phase. While a significant degree of supercooling or $HCl_{(g)}$
512 supersaturation during condensation would request the use of kinetic fractionation
513 factors, equilibrium fractionation factors can be used in the theoretical framework of
514 condensation at thermodynamical equilibrium. Using the calculated fractionation
515 factors, it appears that the condensation of halite can lead to a significant enrichment in
516 ^{37}Cl of the residual $HCl_{(g)}$, which is fractionated by more than +3 ‰ with respect to the
517 starting nebular composition for a condensed fraction above 90 % (Fig. 9). At this point

40% of nebular chlorine is locked in chlorapatite and 50% in halite, while 10% is still present as $HCl_{(g)}$. The fractionation reaches more than +5.5 ‰ for a condensed fraction above 98 % (in this case halite now accounts for 58% of total nebular chlorine and only less than 2% are still present as $HCl_{(g)}$). Later interaction of chondrites with heavier HCl at lower temperature, still under gas state or condensed as hydrates, could lead to both their acidic alteration (Zolotov and Miromenko, 2007) and isotopic enrichment in ^{37}Cl as proposed by Sharp et al. (2016).

The present scenario relies on an efficient condensation of halite as the source of isotopic fractionation between nebular gas and chondrites and is only based on equilibrium fractionation processes. However, the origin of halite in chondrites remains unclear and more complex processes are likely involved. As for chlorapatite and sodalite, halite probably formed during brine circulations on the parent bodies (Zolensky et al., 1999, Whitby et al., 2000, Bridges et al., 2004) but some halite crystals and their fluid inclusions have H and O isotopic systematics indicating preservation of pristine nebular volatiles (Yurimoto et al., 2014). While the low Cl abundance in chondrites (less than 10% of the solar Cl based on Clay et al. 2017) does not favor efficient condensation of halite, we note that the Cl isotopic compositions of halite in the Zag ordinary chondrite (-2.8‰ ≤ $\delta^{37}Cl$ ≤ -1.4‰, Bridges et al., 2004) and sodalite in carbonaceous chondrites inclusions (-2.1‰ ≤ $\delta^{37}Cl$ ≤ -0.4‰, Sharp et al., 2007) are well in line with the composition expected in our Rayleigh distillation model.

5- Conclusion

In the present work, a consistent set of theoretical $^{37}Cl/^{35}Cl$ β-factors has been computed for selected minerals and molecules at the density functional theory level. The

β-factor is an intrinsic property of the phases, defined with respect to an ideal system. They are not directly accessible from experiment but their computation makes it possible to relate the isotopic fractionation properties to local chemical bonding and to disentangle the contribution of individual phases in equilibrium isotopic fractionation processes.

The present results reveal the important role of solution chemistry on the isotopic fractionation of chlorine during the precipitation of chloride salts from aqueous solutions. They also suggest that the variability of chlorine isotopic composition observed in objects of the solar system could be inherited from Rayleigh fractionation processes during the nebula condensation.

Accordingly, further works should aim at developing efficient modeling methods able to treat large systems such as chemically complex aqueous solutions and their interfaces with solids at the best approximation level. The present results could also motivate experimental works on isotopic fractionation processes during the high-temperature condensation of solids and further measurements of Cl isotopic composition in mineral paragenesis of primitive meteorites.

References

Agron, P.A., Busing, W.R., 1985. Magnesium dichloride hexahydrate, $MgCl_2*6H_2O$, by neutron diffraction. Acta Cryst. C41, 8-10.

Agron, P.A., Busing, W.R., 1986. Calcium and strontium dichloride hexahydrates by neutron diffraction. Acta Cryst. C 42, 141–143

566 Aufort, J., Ségalen, L., Gervais, C., Paulatto, L., Blanchard, M., Balan, E., 2017. Site-specific
567 equilibrium isotopic fractionation of oxygen, carbon and calcium in apatite.
568 Geochim. Cosmochim. Acta 219, 57-73.
569 Balan, E., Ingrin, J., Delattre, S., Kovacs, I., Blanchard, M., 2011a. Theoretical infrared
570 spectrum of OH-defects in forsterite. Eur. J. Mineral. 23, 285–292.
571 Balan, E., Delattre, S., Roche, D., Segalen, L., Morin, G., Guillaumet, M., Blanchard, M.,
572 Lazzeri, M., Brouder, C., Salje, E.K.H. 2011b. Line-broadening effects in the
573 powder infrared spectrum of apatite, Phys. Chem. Minerals 38, 111-122.
574 Balan, E., Blanchard, M., Pinilla, C., Lazzeri, M., 2014. First-principles modeling of sulfate
575 incorporation and $^{34}S/^{32}S$ isotopic fractionation in different calcium carbonates.
576 Chem. Geol. 374–375, 84-91
577 Balan, E., Blanchard, M., Lazzeri, M., Ingrin, J., 2017. Theoretical Raman spectrum and
578 anharmonicity of tetrahedral OH defects in hydrous forsterite. Eur. J. Mineral. 29,
579 201-212.
580 Balan, E., Noireaux, J., Mavromatis, V., Saldi, G.D., Montouillout, V., Blanchard, M.,
581 Pietrrucci, F., Gervais, C., Rustad, J.R., Schott, J., Gaillardet, J. 2018. Theoretical
582 isotopic fractionation between structural boron in carbonates and aqueous boric
583 acid and borate ion. Geochim. Cosmochim. Acta 222, 117-129.
584 Barnes, J.D., Cisneros, M., 2012. Mineralogical control on the chlorine isotope
585 composition of altered oceanic crust. Chem. Geol. 326–327, 51–60.
586 Barnes, J.D., Sharp, J.D., 2017. Chlorine isotope geochemistry. Reviews in Mineralogy &
587 Geochemistry 82, 345-378.
588 Baroni, S., de Gironcoli, S., Dal Corso, A., Giannozzi, P., 2001. Phonons and related crystal
589 properties from density-functional perturbation theory. Reviews of Modern
590 Physics 73, 515-561.

591 Beyer, C., Klemme, S., Wiedenbeck, M., Stracke, A., Vollmer, C., 2012. Fluorine in
592 nominally fluorine-free mantle minerals: experimental partitioning of F between
593 olivine, orthopyroxene and silicate melts with implications for magmatic
594 processes. Earth Planet. Sci. Lett. 337–338, 1–9.
595 Bigeleisen, J., Mayer, M.G., 1947. Calculation of equilibrium constants for isotopic
596 exchange reactions. J. Chem. Phys. 15, 261-267.
597 Blanchard, M., Poitrasson, F., Méheut, M., Lazzeri, M., Mauri, F., Balan E., 2009. Iron
598 isotope fractionation between pyrite (FeS_2), hematite (Fe_2O_3) and siderite ($FeCO_3$):
599 a first-principles density-functional theory study. Geochim. Cosmochim. Acta 73,
600 6565-6578.
601 Blanchard, M., Balan, E., Schauble, E., 2017. Equilibrium fractionation of non-traditional
602 isotopes: A molecular modeling perspective. Reviews in Mineralogy and
603 Geochemistry 82, 27-63.
604 Blanchard, M., Méheut, M., Delon, L., Poirier, M., Micoud, P., Le Roux, C., Martin, F., 2018.
605 Infrared spectroscopic study of the synthetic Mg-Ni talc series. Phys. Chem.
606 Minerals 45, 843-854.
607 Bonifacie, M., Busigny, V., Mevel, C., Philippot, P., Agrinier, P., Jendrzejewski, N.,
608 Scambellui, M., Javoy, M., 2008. Chlorine isotopic composition in seafloor
609 serpentinites and high-pressure metaperidotites. Insights into oceanic
610 serpentinization and subduction processes. Geochim. Cosmochim. Acta 72, 126–
611 139.
612 Bouvier, A., Manzini, M., Rose-Koga, E., Nichols, A.R.L. 2019. Tracing of Cl input into the
613 sub-arc mantle through the combined analysis of B, O and Cl isotopes in melt
614 inclusions. Earth Planet. Sci. Lett. 507, 30-39.

615 Bridges, J., Banks, D.A., Smith, M., Grady, M.M., 2004. Halite and stable chlorine isotopes
616 in the Zag H3-6 breccia. Meteor. Planet. Sci. 39, 657-666.
617 Cisneros, M. 2013. An experimental calibration of chlorine isotope fractionation
618 between amphibole and fluid at 700 °C and 0.2 GPa. M.S. Thesis, University of
619 Texas at Austin.
620 Clay, P.L., Burgess, R., Busemann, H., Ruzie-Hamilton, L., Joachim, B., Day, J.M.D.,
621 Ballentine, C.J., 2017. Halogens in chondritic meteorites and terrestrial accretion.
622 Nature 551, 614-618.
623 Corno, M., Busco, C., Civalleri, B., Ugliengo, P., 2006. Periodic ab initio study of structural
624 and vibrational features of hexagonal hydroxyapatite Ca10(PO4)6(OH)2. Phys.
625 Chem. Chem. Phys. 8, 2464–2472.
626 Crépisson, C., Blanchard, M., Bureau, H., Sanloup, C., Withers, A.C., Khodja, H., Surblé, K.,
627 Béneut, K., Leroy, C., Giura, P., Balan, E., 2014).Clumped fluoride-hydroxyl defects
628 in forsterite: Implications for the upper mantle. Earth Planet. Sci. Lett. 390, 287-
629 295.
630 Crépisson, C., Blanchard, M., Lazzeri, M., Balan, E., Sanloup, C., 2018. New constraints on
631 Xe incorporation mechanisms in olivine from first-principles calculations.
632 Geochim. Cosmochim. Acta 222, 146-155.
633 Czarnacki, M., Halas, S., 2012. Isotope fractionation in aqua-gas systems: Cl_2–HCl–Cl^-,
634 Br_2–HBr–Br^- and H_2S–S^{2-}. Isotopes in Environmental and Health Studies 45, 55–64.
635 Dalou, C., Koga, K.T., Shimizu, N., Boulon, J., Devidal, J.L., 2012. Experimental
636 determination of F and Cl partitioning between lherzolite and basaltic melt. Cont.
637 Mineral. Petro. 163, 591–609.
638 Dhooghe, F., De Keyser, J., Altwegg, K., Briois, C., Balsiger, H., Berthelier, J.-J., Calmonte, U.,
639 Cessateur, G., Combi, M.R., Equeter, E., Fiethe, B., Fray, N.,Fuselier, S., Gasc, S.,

640 Gibbons, A., Gombosi, T., Gunell, H., Hässig, M., Hilchenbach, M., Le Roy, L.,
641 Maggiolo, R., Mall, U., Marty, B., Neefs, E., Rème, H., Rubin, M., Sémon, T., Tzou, C.-Y.,
642 Wurz, P., 2017. Halogens as tracers of protosolar nebula material in comet
643 67P/Churyumov-Gerasimenko. Monthly Notices of the Royal Astronomical Society
644 472, 1336-1345.
645 Downs, R.T., Hall-Wallace, M., 2003. The American Mineralogist Crystal Structure
646 Database. Amer. Mineral. 88, 247-250
647 Ducher, M., Blanchard, M., Balan, E., 2016. Equilibrium zinc isotope fractionation in Zn-
648 bearing minerals from first-principles calculations. Chem. Geol. 443, 87-96.
649 Eggenkamp, H.G.M., Kreulen, R., Koster van Groos, A.F., 1995. Chloride stable isotope
650 fractionation in evaporites. Geochim. Cosmochim. Acta 59, 5169–5175.
651 Eggenkamp, H.G.M., 2014. The geochemistry of stable chlorine and bromine isotopes.
652 Springer, Berlin
653 Eggenkamp, H.G.M., 2015b. Comment on "Stable isotope fractionation of chlorine during
654 the precipitation of single chloride minerals "by Luo, C.-g., Xiao, Y.-k., Wen, H.-j., Ma,
655 H.-z., Ma, Y.-q., Zhang, Y.-l., Zhang, Y.-x. And He, M.-y. [Applied Geochemistry 47
656 (2014) 141-149]. Appl. Geochem. 54, 111–116.
657 Eggenkamp, H.G.M., Bonifacie, M., Ader, M., Agrinier, P., 2016. Experimental
658 determination of stable chlorine and bromine isotope fractionation during
659 precipitation of salt from a saturated solution. Chem. Geol. 433, 46-56.
660 Fegley, B. Jr., Lewis, J.S., 1980. Volatile element chemistry in the solar nebula: Na, K, F, CI,
661 Br, and P. Icarus 41, 439-455.
662 Friesen, S., Hefter, G., Buchner, R., 2019. Cation hydration and ion pairing in aqueous
663 solutions of $MgCl_2$ and $CaCl_2$. J. Phys. Chem. B 123, 891-900.

Fujino, K., Sasaki, S., Takeuchi, Y., Sadanaga, R., 1981. X-ray determination of electron distributions in forsterite, fayalite and tephroite. Acta Cryst. B 37, 513–518.

Ganino, C., Libourel, G., (2017) Reduced and unstratified crust in CV chondrite parent body. Nature Comm. 8, 261.

Gargano; A.M., Sharp, Z.D., Taylor, L.A., 2017. Further constraining the chlorine isotope composition of the solar nebula: main group iron meteorites. 80th Annual meeting of the Meteoritical Society (LPI contrib. N°1987), abstract#6141.

Giannozzi, P., Baroni, S., Bonini, N., Calandra, M., Car, R., Cavazzoni, C., Ceresoli, D., Chiarotti, G.L., Cococcioni, M., Dabo, I., Dal Corso, A., de Gironcoli, S., Fabris, S., Fratesi, G., Gebauer, R., Gerstmann, U., Gougoussis, C., Kokalj, A., Lazzeri, M., Martin-Samos, L., Marzari, N., Mauri, F., Mazzarello, R., Paolini, S., Pasquarello, A., Paulatto, L., Sbraccia, C., Scandolo, S., Sclauzero, G., Seitsonen, A.P., Smogunov, A., Umari, P., Wentzcovitch, R.M., 2009. Quantum ESPRESSO: a modular and open-source software project for quantum simulations of materials. Journal of Physics: Condensed Matter 21, 395502.

Giunta, T., Labidi, J., Eggenkamp, H.G.M., 2017. Chlorine isotope fractionation between chloride (Cl^-) and dichlorine (Cl_2). Geochim. Cosmochim. Acta 213, 375–382.

Godon, A., Jendrzejewski, N., Castrec-Rouelle, M., Dia, A., Pineau, F., Boulègue, J., Javoy, M., 2004. Origin and evolution of fluids from mud volcanos in the Barbados accretionary complex. Geochim. Cosmochim. Acta 68, 2153–2165.

Gregorkiewitz, M., Lebech, B., Mellini, M., Viti, C., 1996. Hydrogen positions and thermal expansion in lizardite-1T from Elba: A low-temperature study using Rietveld refinement of neutron diffraction data. Amer. Mineral. 81, 1111–1116.

Hamann, D.R., 2013. Optimized norm-conserving Vanderbilt pseudopotentials. Phys. Rev. B 88, 085117.

689 Hassan, I., Antao, S.M., Parise, J.B., 2004. Sodalite: High-temperature structures obtained
690 from synchrotron radiation and Rietveld refinements. Amer. Mineral. 89 359-
691 364.
692 Hendricks, S., Jefferson, M., Mosley, V. 1932. The crystal structures of some natural and
693 synthetic apatite-like substances. Zeit. Kristall. 81, 352-369.
694 Hoering, T.C., Parker, P.L., 1961. The geochemistry of the stable isotopes of chlorine.
695 Geochim. Cosmochim. Acta 23, 186–199.
696 Hönnerscheid, A., Nuss, J., Mühle, C., Jansen, M., 2003. Die kristallstrukturen der
697 monohydrate von lithiumchlorid und lithiumbromid. Zeit. anorganische und
698 allgemeine Chem. 629, 312-316.
699 Javoy, M., Balan, E., Méheut, M., Blanchard, M., Lazzeri, M., 2012. First-principles
700 investigation of equilibrium isotopic fractionation of O- and Si-isotopes between
701 refractory solids and gases in the solar nebula. Earth Planet. Sci. Lett. 319/320,
702 118-127.
703 Joachim, B., Pawley, A., Lyon, I.C., Marquardt, K., Henkel, T., Clay, P.L., Ruzié, L., Burgess,
704 R., Ballentine, C.J., 2015. Experimental partitioning of F and Cl between olivine,
705 orthopyroxene and silicate melt at Earth's mantle conditions. Chem. Geol. 416,
706 65–78.
707 Joachim, B., Stechern, A., Ludwig, T., Konzett, J., Pawley, A., Ruzie-Hamilton, L., Clay, P.L.,
708 Burgess, R., Ballentine, C.J., 2017. Effect of water on the fluorine and chlorine
709 partitioning behavior between olivine and silicate melt. Contrib. Mineral. Petrol.
710 172, 15.
711 Kama, M., Caux, E., Lopez-Sepulcre, A., Wakelam, V., Dominik, D., Ceccarelli, C., Lanza, M.,
712 Lique, F., Ochsendorf, B.B., Lis, D.C., Caballero, R.N., Tiellens, A.G.G.M., 2015.

713 Depletion of chlorine into HCl ice in a protostellar core: The CHESS spectral
714 survey of OMC-2 FIR 4. Astronomy Astrophysics 574, A107.
715 Kendrick, M.A., Scambelluri, M., Honda, M., Phillips, D., 2011. High abundances of noble
716 gas and chlorine delivered to the mantle by serpentinite subduction. Nature Geos.
717 4, 807–812.
718 Kusebauch, C., John, T., Whitehouse, M.J., Engvik, A.K. 2015. Apatite as probe for the
719 halogen composition of metamorphic fluids (Bamble Sector, SE Norway). Contrib.
720 Mineral. Petrol. 170, 34.
721 Lodders, K., 2003. Solar system abundances and condensation temperatures of the
722 elements. Astrophysical J. 591, 1220–1247.
723 Lundgren, J.-O., Olovsson, I., 1967. Hydrogen bond studies. XV. The crystal structure of
724 hydrogen chloride dihydrate. Acta Cryst. 23, 966-971.
725 Luo, C.G., Xiao, Y.K., Wen, H.J., Ma, H.H., Ma, Y.Q., Zhang, Y.L., Zhang, Y.X., He, M.Y., 2014.
726 Stable isotope fractionation of chloride during the precipitation of single chloride
727 minerals. Appl. Geochem. 47, 141–149.
728 Luo, C.G., Xiao, Y.K., Wen, H.J., Ma, H.H., Ma, Y.Q., Zhang, Y.L., He, M.Y., 2015. Reply to the
729 comment on the paper “Stable isotope fractionation of chlorine during the
730 precipitation of single chloride minerals”. Appl. Geochem. 54, 117–118.
731 Méheut, M., Lazzeri, M., Balan, E., Mauri, F., 2007. Equilibrium isotopic fractionation
732 between kaolinite, quartz and water: prediction from first-principles density-
733 functional theory. Geochim. Cosmochim. Acta 71, 3170-3181.
734 Moynier, F., Yin, Q.-Z., Schauble, E., 2011. Isotopic evidence of Cr partitioning into Earth's
735 core. Science 331,1417-1420.
736 Padmanabhan, V., Busing, W., Levy, H., 1978. Barium chloride dihydrate by neutron
737 diffraction. Acta Cryst. B34, 2290-2292.

738 Perdew, J.P., Burke, K., Ernzerhof, M., 1996. Generalized Gradient Approximation Made
739 Simple. Phys. Rev. Lett. 77, 3865–3868.
740 Perdew, J.P., Ruzsinszky, A., Csonka, G.I., Vydrov, O.A., Scuseria, G.E., Constantin, L.A.,
741 Zhou, X., Burke, K., 2008. Restoring the density-gradient expansion for exchange
742 in solids and surfaces. Phys. Rev. Lett. 100, 136406.
743 Pham, V.-T., Fulton, J.L., 2013. Ion-pairing in aqueous $CaCl_2$ and RbBr solutions:
744 Simultaneous structural refinement of XAFS and XRD data. J. Chem. Phys. 138,
745 044201.
746 Pham, V.-T., Fulton, J.L., 2016. High-resolution measurement of contact ion-pair
747 structures in aqueous RbCl solutions from the simultaneous corefinement of
748 their Rb and Cl K- edge XAFS and XRD spectra, J. Sol. Chem. 45, 1061–1070.
749 Pham, V.-T., Fulton, J. L., 2018. Contact ion-pair structure in concentrated cesium
750 chloride aqueous solutions: An extended X-ray absorption fine structure study. J.
751 Electron Spectro. and Related Phenom. 229, 20-25.
752 Reissland, J.A., 1973. The physics of phonons (John Wiley and sons LTD, London-New
753 York- Sydney-Toronto, 1973)
754 Richet, P., Bottinga, Y., Javoy M., 1977. A review of hydrogen, carbon, nitrogen, oxygen,
755 and chlorine stable isotope fractionation among gaseous molecules. Annual
756 Reviews of Earth and Planetary Sciences 5, 65–110.
757 Rustad, J. R., Zarzycki, P., 2008. Calculation of site-specific carbon-isotope fractionation
758 in pedogenic oxide minerals. PNAS 105, 0297–10301.
759 Scambelluri, M., Müntener, O., Ottolini, L., Pettke, T.T., Vannucci, R., 2004. The fate of B, Cl
760 and Li in the subducted oceanic mantle and in the antigorite breakdown fluids.
761 Earth Planet. Sci. Lett. 222, 217–234.

762 Schauble, E.A., Rossman, G.R., Taylor, H.P., 2003. Theoretical estimates of equilibrium
763 chlorine-isotope fractionations. Geochim. Cosmochim. Acta 67, 3267-3281.
764 Schauble, E.A., Ghosh, P., Eiler, J.M., 2006. Preferential formation of $^{13}C–^{18}O$ bonds in
765 carbonate minerals, estimated using first-principles lattice dynamics. Geochim.
766 Cosmochim. Acta 70, 2510-2529.
767 Schauble, E.A., Sharp, Z.D., 2011. Modeling isotopic signatures of nebular chlorine
768 condensation. Goldschmidt Conference Abstracts, Mineral. Mag. 21, 1810.
769 Schaefer, L., Fegley, B., Jr., 2010. Cosmochemistry pp. 347–377, In Principles and
770 Perspectives in Cosmochemistry: Lecture Notes of the Kodai School on "Synthesis
771 of Elements" Eds. A. Goswami and B.E. Reddy, Springer.
772 Schlipf, M., Gygi, F. 2015. Optimization algorithm for the generation of ONCV
773 pseudopotentials. Computer Physics Communications 196, 36.
774 Shannon, R.D., 1976. Revised effective ionic radii and systematic studies of interatomic
775 distances in halides and chalcogenides", Acta Cryst. A32, 751-767.
776 Sharp, Z.D., Barnes, J.D., 2004. Water soluble chlorides in massive seafloor serpentinites:
777 a source of chloride in subduction zones. Earth Planet Sci Lett 226, 243–254.
778 Sharp, Z.D., Barnes, J.D., Brearley, A.J., Chaussidon, M., Fischer, T.P., Kamenetsky, V.S.,
779 2007. Chlorine isotope homogeneity of the mantle, crust and carbonaceous
780 chondrites. Nature 446, 1062−1065.
781 Sharp, Z.D., Shearer, C.K., McKeegan, K.D., Barnes, J.D., Wang, Y.Q., 2010a. The chlorine
782 isotope composition of the Moon and implications for an anhydrous mantle.
783 Science 329, 1050–1053.
784 Sharp, Z.D., Barnes, J.D., Fischer, T.P., Halick, M., 2010b. A laboratory determination of
785 chlorine isotope fractionation in acid systems and applications to volcanic
786 fumaroles. Geochim. Cosmochim. Acta 74, 264–273.

787 Sharp, Z.D., Mercer, J.A., Jones, R.H., Brearley, A.J., Selverstone, J., Bekker, A., Stachel, T.,
788 2013. The chlorine isotopic composition of chondrites and Earth. Geochim.
789 Cosmochim. Acta 107, 189-204
790 Sharp ZD, Williams J, Shearer CK, Jr., Agee CB, McKeegan KD (2016) The chlorine isotope
791 composition of Martian meteorites 2. Implications for the early solar system and
792 the formation of Mars. Meteor. Planet. Sci., 51, 2111-2126.
793 Sirdeshmukh, D.B., Sirdeshmukh, L., Subhadra, K.G., 2001. Alkali halides A handbook of
794 physical properties, Springer, Berlin.
795 Volfinger, M., Robert, J.-L., Vielzeuf, D., Neiva, A.M.R., 1985. Structural control of the
796 chlorine content of OH-bearing silicates (micas and amphiboles). Geochim.
797 Cosmochim. Acta 49, 37–48.
798 Wang, Y., Hsu, W., Guan, Y., 2019. An extremely heavy chlorine reservoir in the Moon:
799 Insights from the apatite in lunar meteorites. Scientific Rep. 9, 5727.
800 Whitby, J., Burgess, R., Turner, G., Gilmour, J., Bridges, J., 2000. Extinct ^{129}I in halite from
801 a primitive meteorite: evidence for evaporite formation in the early solar system.
802 Science 288, 1819-1821.
803 Wood, B.J., Smythe, D., Harrison, T. 2019. The condensation temperatures of the
804 elements: a reappraisal. Amer. Mineral. *in the press*
805 Wyckoff, R.W.G, 1963. Crystal Structures 1 pp 239-444 Second edition. Interscience
806 Publishers, New York, New York
807 Yurimoto, H., Itoh, S., Zolensky, M., Kusakabe, M., Karen, A., Bodnar, R., 2014. Isotopic
808 compositions of asteroidal liquid water trapped in fluid inclusions of chondrites.
809 Geoch. J. 48, 549-560.

Zolensky, M.E., Bodnar, R.J., Gibson, E.K. Jr, Nyquist, L.E., Reese, Y., Shih, C.-Y., Wiesmann, H., 1999. Asteroidal water within fluid inclusion-bearing halite in an H5 chondrite, Monahans. Science 285, 1377-1379.

Zolotov, M.Y., Mironenko, M.V., 2007 Hydrogen chloride as a source of acid fluids in parent bodies of chondrites. Lun. Planet. Sci. Conf. 38, 2340.

Figure captions:

Figure 1: Reduced partition function ratio of $HCl_{(g)}$, $Cl_{2(g)}$, halite ($NaCl_{(c)}$), sylvite ($KCl_{(c)}$) and $RbCl_{(c)}$. Continuous lines: this study; dotted lines: Schauble et al. 2003; dashed lines: Richet al. 1977. Inset: comparison of β-factors at 0°C.

Figure 2: Comparison of theoretical and experimental vibrational frequencies in Cl_2 molecule and alkaline chlorides.

Figure 3: Theoretical β-factors at 22°C of anhydrous (full circles) and hydrated (empty circles) chloride salts as a function of the cationic radius. Note the correlation observed for the anhydrous salts and the weak variations of β-factors observed among the series of hydrated salts. Ionic radii from Shannon (1976) for cations in 6-fold coordination, excepted Cs and Ba (8-fold coordination).

Figure 4: Theoretical β-factors of minerals for temperatures above 450 K. Note the higher values observed for substitutional Cl in silicates. The less stable forsterite models (Si_Cl2, Mg_Cl2, Mg_Cl3 and Mg_Cl4) are not displayed.

Figure 5: Comparison of empirical and theoretical β-factors at 22°C. Full and empty circles correspond to anhydrous and hydrated salts, respectively. Note the larger and systematic discrepancy observed for the heavier alkaline chlorides. The size of the symbols corresponds to an error bar of +/- 0.1 ‰. The error bar on the empirical β-factor of Cl_2 corresponds to that of the Cl_2-Cl^- fractionation factor at 25°C reported by Giunta et al. (2017).

Figure 6: Estimated theoretical β-factor of aqueous chloride ions, obtained by combining the present theoretical β-factors of solids and the fractionation factors reported by Eggenkamp et al. (2016), reported as a function of the ionic potential (Z/r_{ion}) of the associated cation. The highest values, observed for Li and alkaline-earth (Sr, Ca, Mg) counter-cations and averaging to 2.92, likely matches the theoretical β-factor of water coordinated Cl^- ions. Departure from this value is ascribed to the formation of contact ion pairs with large alkaline cations. Estimated errors bars are +/- 0.2 ‰ combining the precision of experimental measurements and theoretical values.

Figure 7: Reduced partition function ratio of $HCl_{(g)}$ and HCl trihydrate. Note the cross-over at 205 K, leading to significant ^{37}Cl enrichment of $HCl_{(g)}$ at temperatures lower than 140 K as previously reported by Schauble and Sharp (2011).

Figure 8: Isotopic fractionation factors between $HCl_{(g)}$ and other Cl-bearing molecules and condensates from the nebular environment. Depending on the condensation models, formation of sodalite at 950 K (Lodders 2003; Fegley and Lewis 1980) only leads to a weak isotopic fractionation of $HCl_{(g)}$ with other phases; whereas a later chlorine condensation as chlorapatite and halite (Schaefer and Fegley 2010) can lead to a more significant ^{37}Cl enrichment of $HCl_{(g)}$ at temperatures between 400 and 500K. Note that the Cl speciation in the nebular gas is dominated by NaCl at 950 K and by HCl at temperatures below 800 K.

Figure 9: Isotopic composition of remaining $HCl_{(g)}$ in a simple scenario of Rayleigh fractionation during chlorine condensation between 500 and 400 K. The chlorapatite

867 accounts for 40% of chlorine condensation. For condensed fraction above 90 %, the
868 remaining $HCl_{(g)}$ is fractionated by more than +3 ‰ with respect to a starting nebular
869 composition of $\delta^{37}Cl$= -3 ‰.
870

871

872 Table 1: Structure and vibrational stretching frequencies of diatomic molecules.
873 Experimental harmonic frequencies (Richet et al. 1977) are indicated in parenthesis.
874

	d (Å)	theo. - exp. (%)	ω ^{35}Cl (cm^{-1})	theo. - exp. (%)	ω ^{37}Cl (cm^{-1})	theo. - exp. (%)
$Cl_{2(g)}$	2.01 (1.98)	+1.5	538.4 (559.7)	-3.8	523.7 (544.4)	-3.8
$HCl_{(g)}$	1.29 (1.27)	+1.6	2888.2(2990.9)	-3.4	2886.0 (2988.7)	-3.4
$NaCl_{(g)}$	2.38		352.7		348.9	
$KCl_{(g)}$	2.67		268.7		264.8	

875
876
877

878 Table 2: Structural and modeling parameters of the investigated crystalline phases. (c),
879 (h), (m) and (o) stand for cubic, hexagonal, monoclinic and orthorhombic crystal
880 systems, respectively.
881

model		crystal syst.	k-point grid	atoms/ cell	cell parameters (Å)	theo. - exp. (%)	ω TO (cm^{-1})	q-point grid
halite	NaCl	(c)	4x4x4	8	a = 5.69 (5.64)[a]	+0.9	154 (164)[a]	4x4x4
sylvite	KCl	(c)	4x4x4	8	a = 6.38 (6.29)[a]	+1.4	129 (142)[a]	4x4x4
	RbCl	(c)	4x4x4	8	a= 6.70 (6.59)[a]	+1.6	102 (116.5)[a]	4x4x4
	CsCl	(c)	6x6x6	2	a= 4.21 (4.12)[a]	+2.1	74 (99.5)[a]	6x6x6
chloromagnesite	$MgCl_2$	(h)	4x4x2	9	a = 3.68 (3.60)[b]	+2.2		4x4x2
					c = 19.62 (17.59)	+11.5		
bischofite	$MgCl_2.6(H_2O)$	(m)	2x2x2	42	a = 9.08 (9.86)[c]	-7.9		1x1x1
					b = 7.39 (7.11)	+3.9		
					c = 6.62 (6.07)	+9.0		
					β = 100.6° (93.7 °)			
	$LiCl.H_2O$	(o)	2x2x2	40	a = 7.69 (7.58)[d]	+1.4		1x1x1
					b = 7.77 (7.68)	+1.2		
					c = 7.64 (7.62)	+0.3		
	$BaCl_2.2(H_2O)$	(m)	2x2x2	36	a = 6.85 (6.72)[e]	+1.9		1x1x1
					b = 11.76 (10.91)	+7.8		
					c = 6.99 (7.13)	-1.9		
					β =90.06° (91.1°)			
	$CaCl_2.6(H_2O)$	(h)	3x3x3	21	a= 7.88 (7.88)[f]	+0.0		2x2x2
					c= 4.04 (3.95)	+2.2		
	$SrCl_2.6(H_2O)$	(h)	3x3x3	21	a= 7.97 (7.96)[f]	+0.0		2x2x2
					c= 4.21 (4.12)	+2.2		
HCl tri-hydrate	$HCl.3(H_2O)$	(m)	3x2x2	32	a = 4.07 (3.99)[g]	+2.0		3x2x2
					b = 12.25 (12.05)	+1.7		
					c = 6.75 (6.70)	+0.7		
					β = 101.1° (100.6 °)			
chlorapatite	$Ca_5(PO_4)_3Cl$	(h)	2x2x2	42	a = 9.86 (9.52)[h]	+3.6		fca
					c = 6.73 (6.85)	-1.7		
sodalite	$Na_8Al_6Si_6O_{24}Cl_2$	(c)	2x2x2	46	a = 8.96 (8.89)[j]	+0.8		fca
anthophyllite	$Mg_7Si_8O_{22}(OH)_2$	(o)	1x1x2	164	a = 18.78 (18.50)[i]	+1.5		fca
					b = 18.14 (17.90)	+1.3		
					c = 5.33 (5.27)	+1.1		
lizardite	$Mg_3Si_2O_5(OH)_4$	(h)	3x3x3	18	a = 5.37 (5.33)[j]	+0.8		fca
					c = 7.35 (7.25)	+1.4		
forsterite	Mg_2SiO_4	(o)	1x1x1		a = 9.60 (9.5)[k]	+1.1		fca
			(2x1x2	112	b = 10.30 (10.19)	+1.1		
			supercell)		c = 12.07 (11.96)	+0.9		

882
883 References: [a]Sirdeshmukh et al. (2001), [b]Wyckoff (1963), [c]Agron and Busing (1985),
884 [d]Hönnerscheid et al. (2003), [e] Padmanabhan et al. (1978), [f]Agron and Busing (1986), [g]Lundgren
885 and Olovsson (1967), [h]Hendricks et al. (1932), [i]Hassan et al. (2004), [j]Gregorkiewitz et al. (1996),
886 [k]Fujino et al. (1981)

887 Table 3: Cl coordination in crystals and relative energy of substitutional Cl-defects.
888

model		Energy* kJ/mol	Coord.	distances (Å)		model	Coord.	distances (Å)
forsterite	Si_Cl1	9.7	3 Mg, 3H	Mg: 2.44, 2 x 2.40	H: 2 x 1.98, 2.0	halite	6 Na	2.84
	Si_Cl1b	4.0	3 Mg, 2H	Mg: 2 x 2.39, 2.48	H: 2 x 1.95	sylvite	6 K	3.19
	Si_Cl2	44.3	3 Mg, 1H	Mg: 2.29, 2 x 2.31	H: 2.08	RbCl	6 Rb	3.35
	Si_Cl3	0	3 Mg, 1H	Mg: 2.33, 2.39, 2.42	H: 2.0	CsCl	8 Cs	3.65
	Mg_Cl1	0	2 Mg, 1Si	Mg: 2.39, 2.40 Si: 2.17		chloromagnesite	3 Mg	2.53
	Mg_Cl2	83.5	2 Mg, 1Si	Mg: 2.43, 2.47 Si: 2.04		bischofite	4 H	2.13, 2.17, 2.21, 2.23
	Mg_Cl3	94.9	2 Mg, 1Si	Mg: 2.41, 2.50 Si: 2.05		HCl tri-hydrate	4 H	2.03, 2.08, 2.11, 2.15
	Mg_Cl4	56.4	2 Mg, 1Si	Mg: 2.40, 2.51 Si: 2.08		chlorapatite	3 Ca	2.79
	Mg_Cl5	2.1	2 Mg, 1Si	Mg: 2.37, 2.51 Si: 2.14		sodalite	4 Na	2.74
lizardite	Cl1	0	3 Mg	2.53		LiCl. H_2O	4 Li, 2H	Li: 2.56, 2x2.67, 2.93 H: 2x2.
	Cl2	47.4	3 Mg	2 x 2.42, 2.46		$BaCl_2.2(H_2O)$	2 H	2.11, 2.18
							2 H	2.12, 2.19
anthophyllite	Cl1	10	3 Mg	2.47, 2 x 2.48		$CaCl_2.6(H_2O)$	6 H	3x2.19, 3x2.28
	Cl2	0	3 Mg	2.45, 2 x 2.5				
						$SrCl_2.6(H_2O)$	6 H	3x2.21, 3x2.26

889 *For each type of defect, the energy is computed with respect to that of the most stable configuration.
890
891

Table 4: Polynomial fits of β-factor of crystals and molecules.

model		a *	$10^6/T^2$ range	model	a *	b *	c*	d*	$10^6/T^2$ range
forsterite	Si_Cl1	0.985	0-5	halite	0.253				0-13.4
	Si_Cl1b	0.944	0-5	sylvite	0.185				0-13.4
	Si_Cl2	1.124	0-5	RbCl	0.162				0-13.4
	Si_Cl3	0.988	0-5	CsCl	0.130				0-13.4
	Mg_Cl1	1.080	0-5	bischofite	0.243				0-13.4
	Mg_Cl2	1.295	0-5	$LiCl.H_2O$	0.272				0-13.4
	Mg_Cl3	1.293	0-5	$BaCl_2.2(H_2O)$	0.263				0-13.4
	Mg_Cl4	1.173	0-5	$CaCl_2.6(H_2O)$	0.263				0-13.4
	Mg_Cl5	1.071	0-5	$SrCl_2.6(H_2O)$	0.254				0-13.4
lizardite	Cl1	0.645	0-5	chloromagnesite	0.471				0-5
	Cl2	0.740	0-5	HCl tri-hydrate	0.319	$-1.993\ 10^{-3}$	$3.951\ 10^{-5}$	$-3.629\ 10^{-7}$	0-45
anthophyllite	Cl1	0.740	0-5	$NaCl_{(g)}$	0.226				0-5
	Cl2	0.725	0-5	$KCl_{(g)}$	0.175				0-5
sodalite		0.234	0-5	$Cl_{2(g)}$	0.6756	$-6.557\ 10^{-3}$	$8.684\ 10^{-5}$	$-8.648\ 10^{-7}$	0-13.4
chlorapatite		0.418	0-5	$HCl_{(g)}$	0.9415	-0.1164	$9.165\ 10^{-3}$	$-2.728\ 10^{-4}$	0-13.4

*The coefficients are defined by the relation: $10^3\ln(\beta)=ax+bx^2+cx^3+dx^4$ where $x=10^6/T^2$ and T is the temperature in Kelvin. Note that quadratic, cubic and quartic coefficients have no physical meaning and simply aim at reproducing the curvature of $10^3\ln(\beta)$ as a function of $10^6/T^2$ for Cl_2, HCl molecule and HCl trihydrate.

903
904
905 Table 5: Theoretical β-factor of chloride salts and Cl_2 molecule at 22 °C.
906

model	1000 ln(β) at 22°C
halite	2.9
sylvite	2.1
RbCl	1.9
CsCl	1.5
bischofite	2.8
$LiCl.H_2O$	3.1
$BaCl_2.2(H_2O)$	3.0
$CaCl_2.6(H_2O)$	3.0
$SrCl_2.6(H_2O)$	2.9
$Cl_{2(g)}$	7.0

907

Figure 1: Reduced partition function ratio of $HCl_{(g)}$, $Cl_{2(g)}$, halite ($NaCl_{(c)}$), sylvite ($KCl_{(c)}$) and $RbCl_{(c)}$. Continuous lines: this study; dotted lines: Schauble et al. 2003; dashed lines: Richet al. 1977. Inset: comparison of β-factors at 0°C.

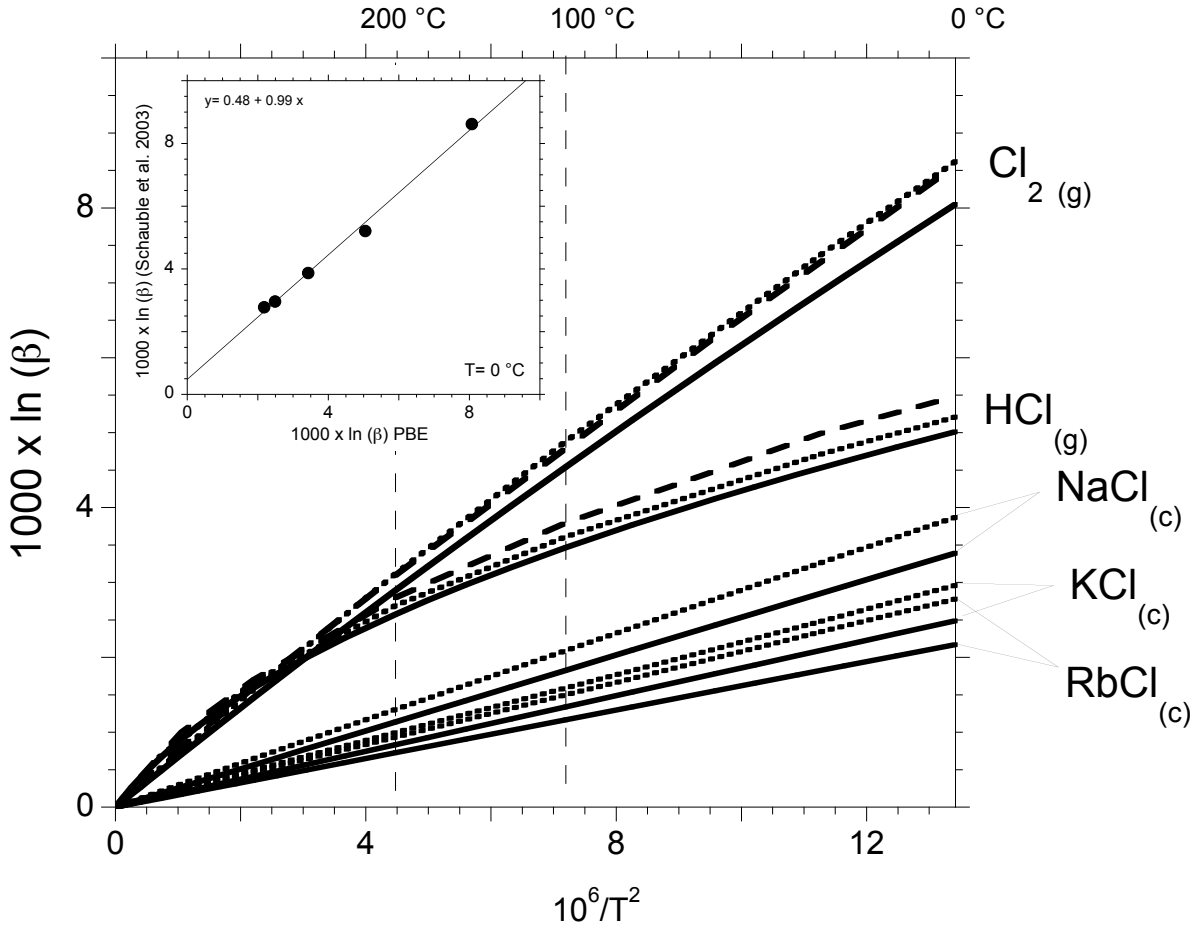

Figure 2: Comparison of theoretical and experimental vibrational frequencies in Cl_2 molecule and alkaline chlorides.

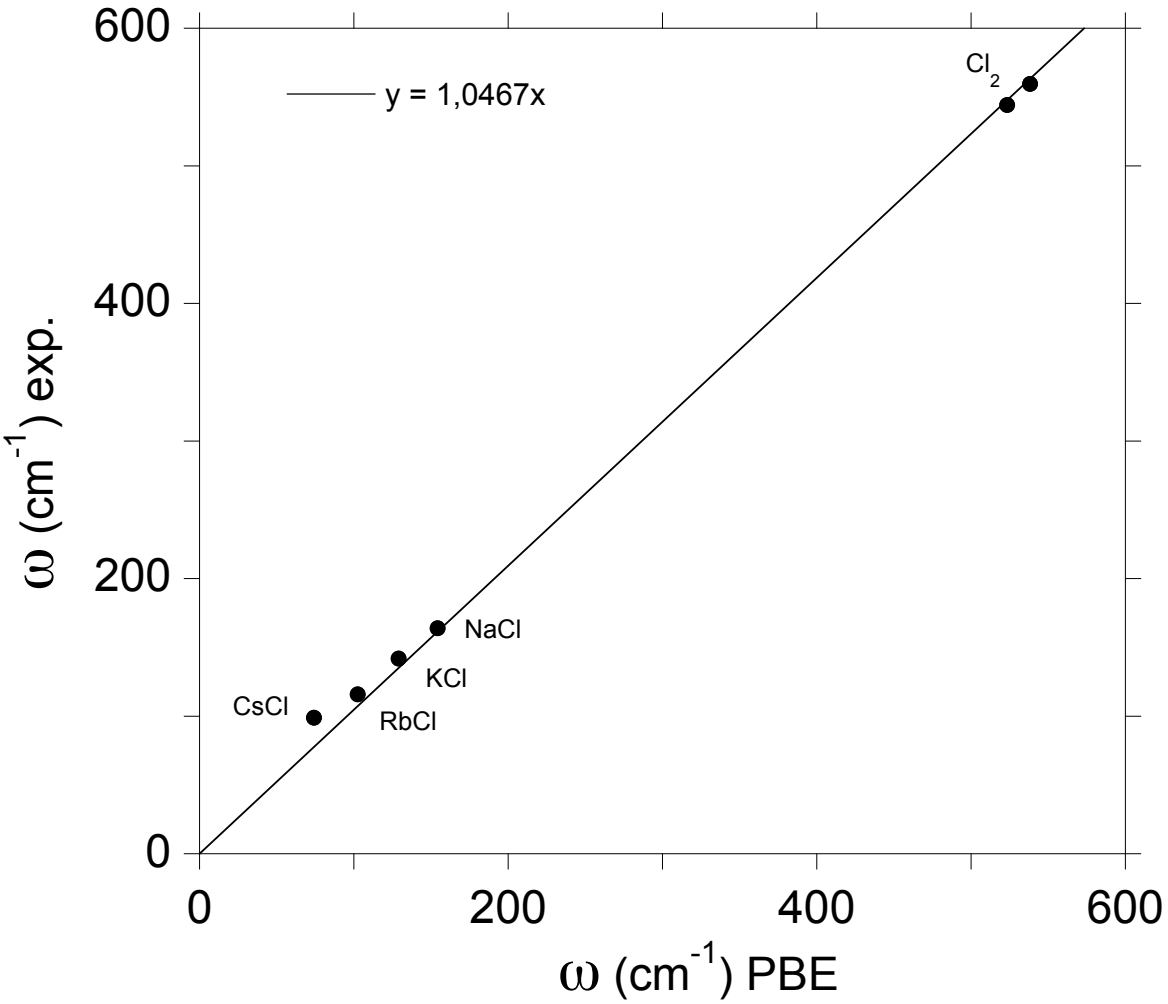

Figure 3: Theoretical β-factors at 22°C of anhydrous (full circles) and hydrated (empty circles) chloride salts as a function of the cationic radius. Note the correlation observed for the anhydrous salts and the weak variations of β-factors observed among the series of hydrated salts. Ionic radii from Shannon (1976) for cations in 6-fold coordination, excepted Cs and Ba (8-fold coordination).

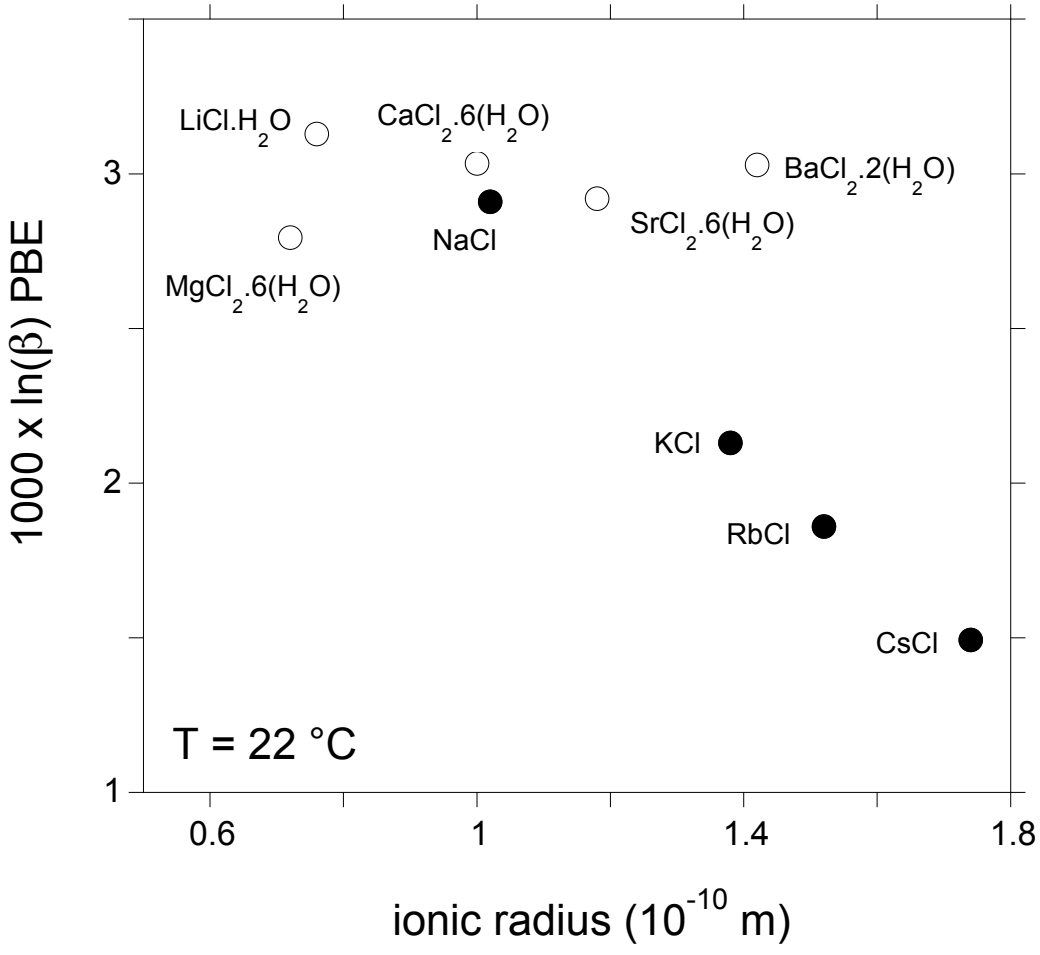

Figure 4: Theoretical β-factors of minerals for temperatures above 450 K. Note the higher values observed for substitutional Cl in silicates. The less stable forsterite models (Si_Cl2, Mg_Cl2, Mg_Cl3 and Mg_Cl4) are not displayed.

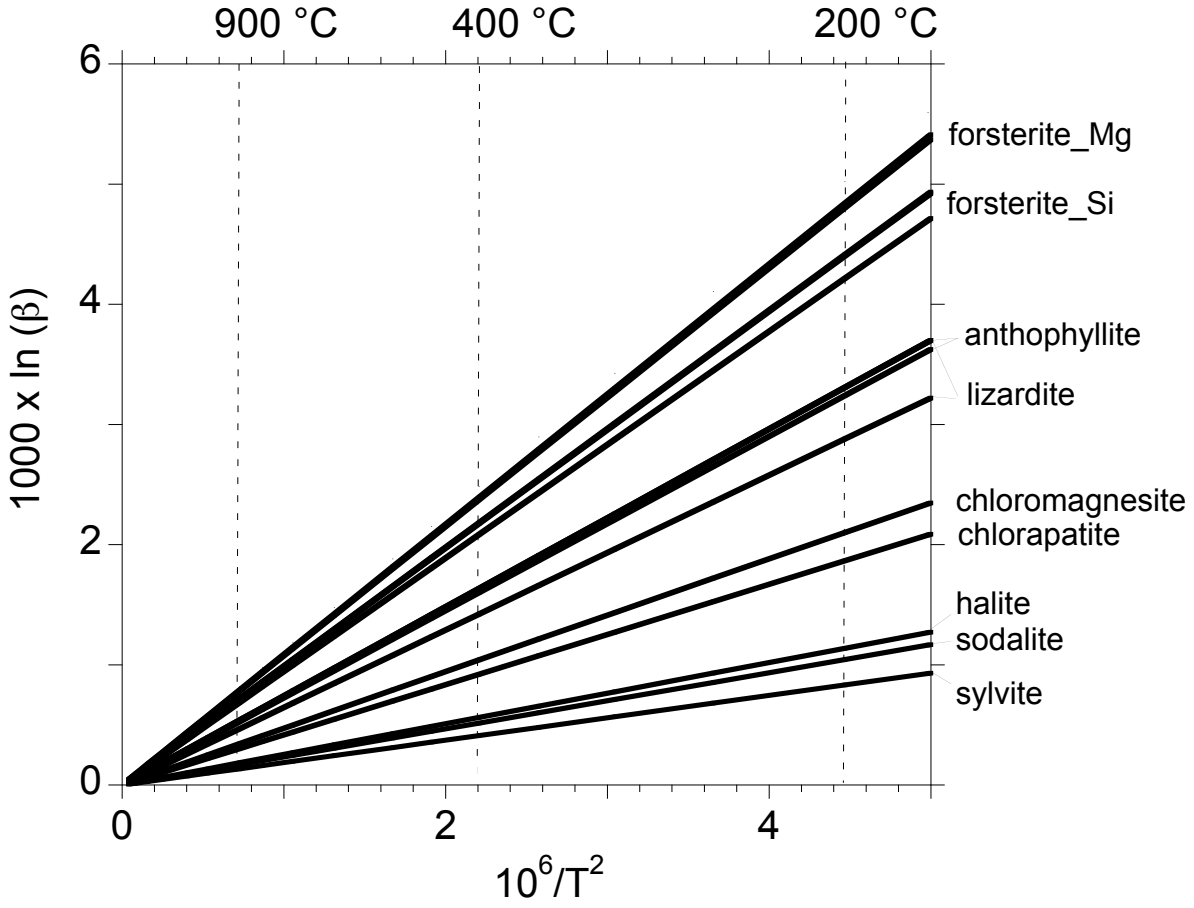

Figure 5: Comparison of empirical and theoretical β-factors at 22°C. Full and empty circles correspond to anhydrous and hydrated salts, respectively. Note the larger and systematic discrepancy observed for the heavier alkaline chlorides. The size of the symbols correspond to error bars of +/- 0.1 ‰. The error bar on the empirical β-factor of Cl_2 corresponds to that of the Cl_2-Cl^- fractionation factor at 25°C reported by Giunta et al. (2017).

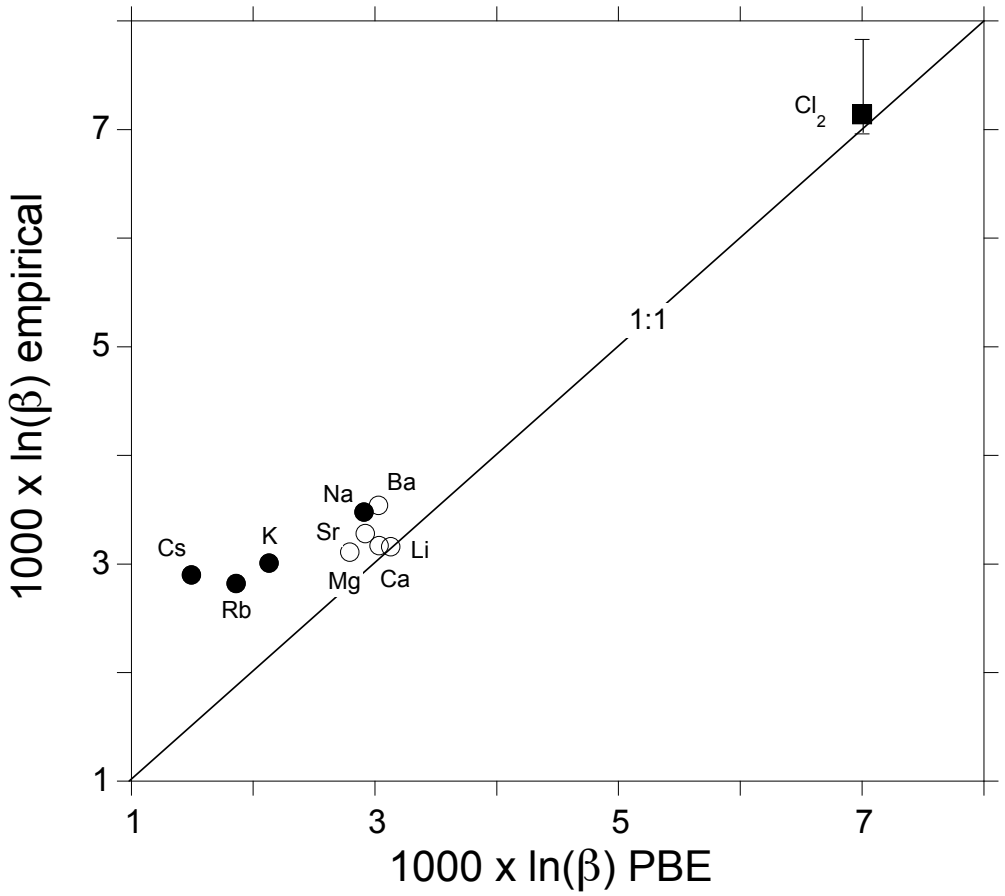

Figure 6: Estimated theoretical β-factor of aqueous chloride ions, obtained by combining the present theoretical β-factors of solids and the fractionation factors reported by Eggenkamp et al. (2016), reported as a function of the ionic potential (Z/r_{ion}) of the associated cation. The highest values, observed for Li and alkaline-earth (Sr, Ca, Mg) counter-cations and averaging to 2.92, likely matches the theoretical β-factor of water coordinated Cl^- ions. Departure from this value is ascribed to the formation of contact ion pairs with large alkaline cations. Estimated errors bars are +/- 0.2 ‰ combining the precision of experimental measurements and theoretical values.

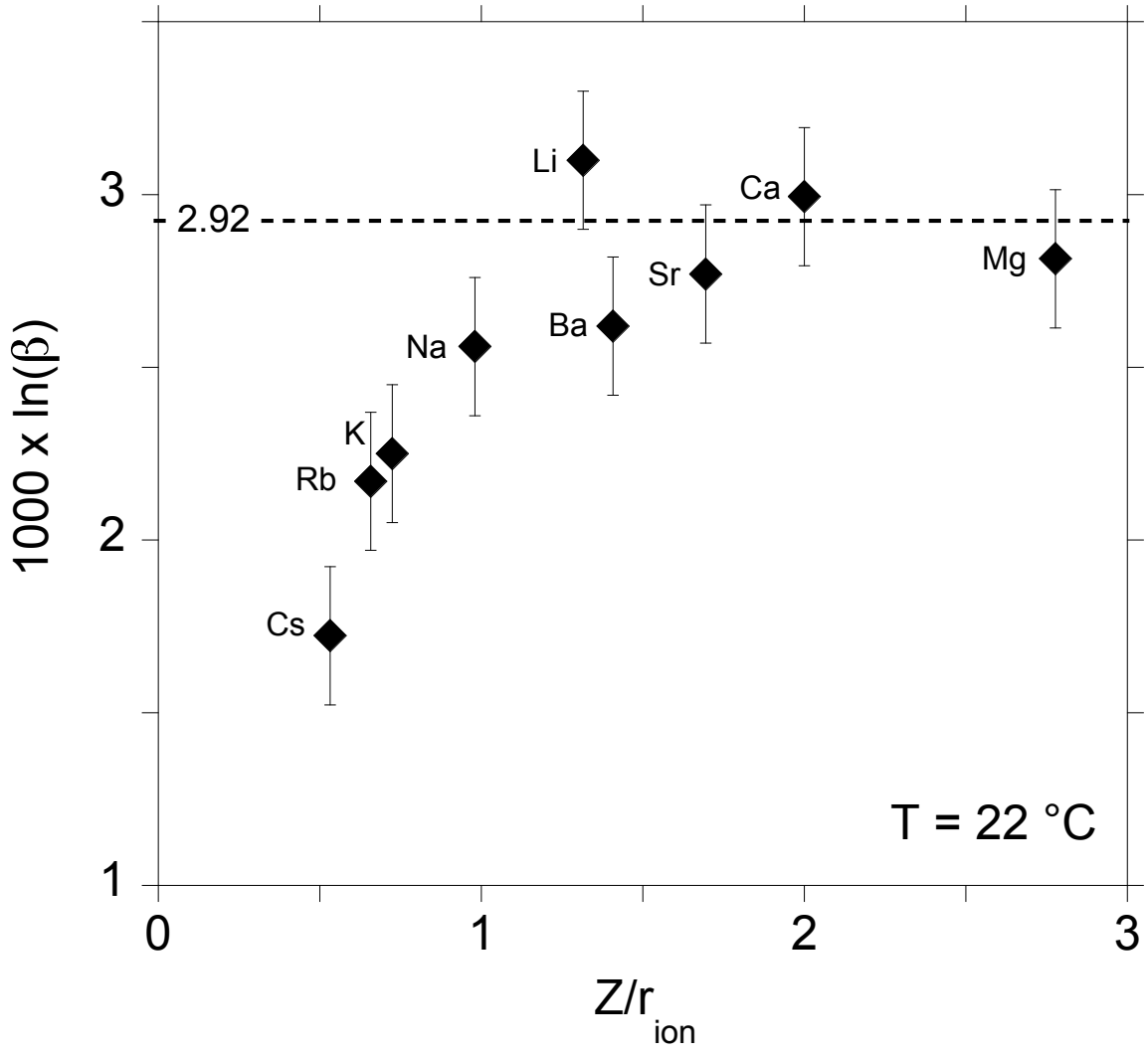

Figure 7: Reduced partition function ratio of $HCl_{(g)}$ and HCl trihydrate. Note the cross-over at 205 K, leading to significant ^{37}Cl enrichment of HCl trihydrate at temperatures lower than 140 K as previously reported by Schauble and Sharp (2011).

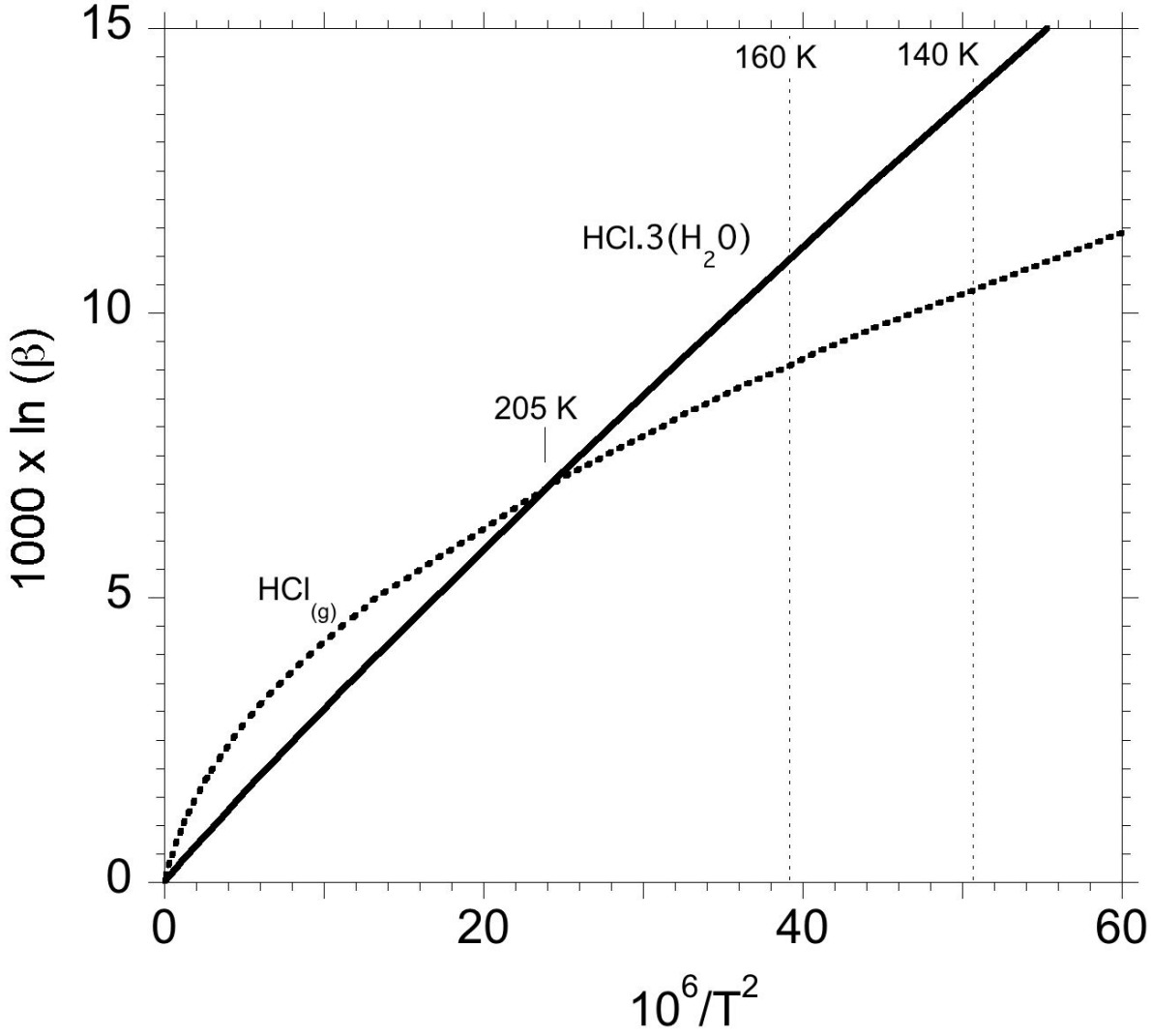

Figure 8: Isotopic fractionation factors between $HCl_{(g)}$ and other Cl-bearing molecules and condensates from the nebular environment. Depending on the condensation models, formation of sodalite at 950 K (Lodders 2003; Fegley and Lewis 1980) only leads to a weak isotopic fractionation of $HCl_{(g)}$ with other phases; whereas a later chlorine condensation as chlorapatite and halite (Fegley and Schaefer 2010) can lead to a more significant ^{37}Cl enrichment of $HCl_{(g)}$ at temperatures between 400 and 500K. Note that the Cl speciation in the nebular gas is dominated by NaCl at 950 K and by HCl at temperatures below 800 K.

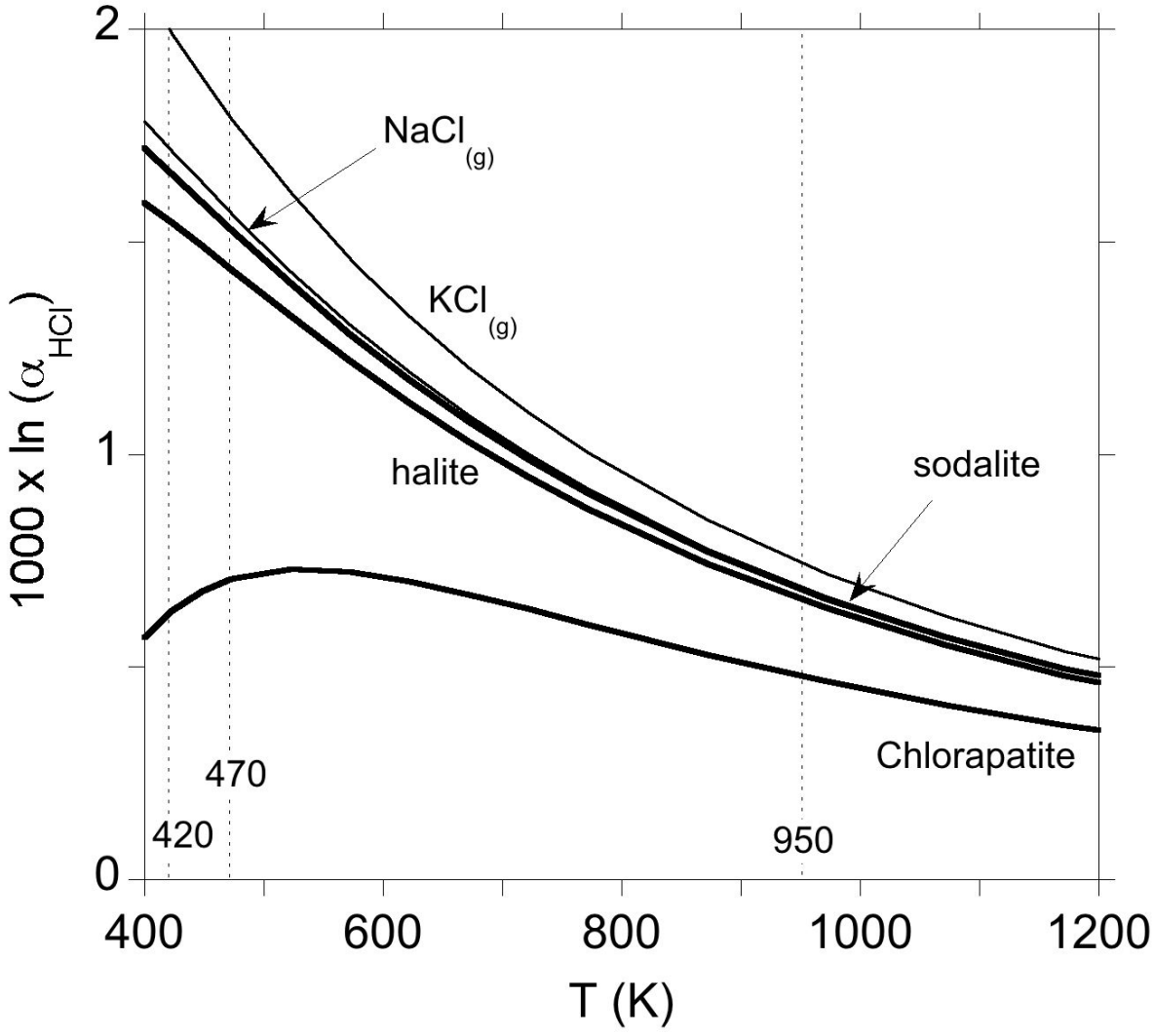

1011 Figure 9: Isotopic composition of remaining $HCl_{(g)}$ in a simple scenario of Rayleigh
1012 fractionation during chlorine condensation between 500 and 400 K. The chlorapatite
1013 accounts for 40% of chlorine condensation. For condensed fraction above 90 %, the
1014 remaining $HCl_{(g)}$ is fractionated by more than +3 ‰ with respect to a starting nebular
1015 composition of $\delta^{37}Cl$= -3 ‰.

1016

1017
1018

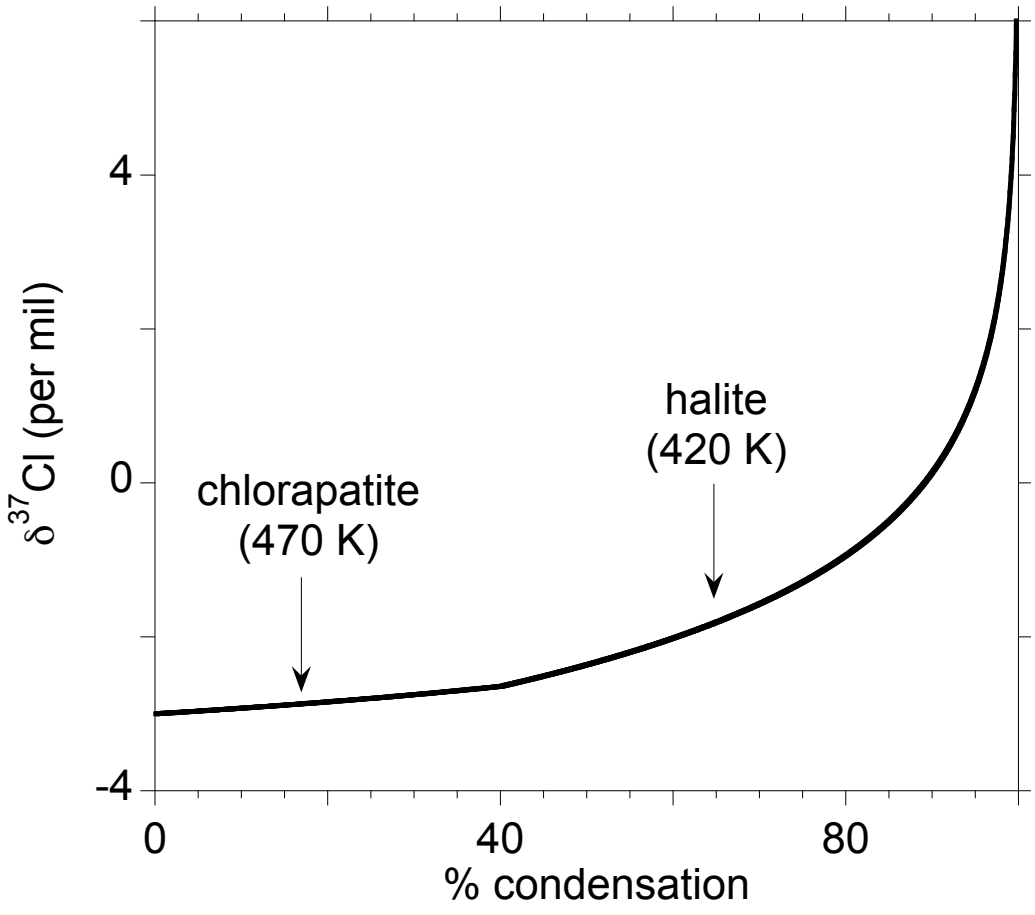

1019